Title:

Brain composition in *Heliconius* butterflies, post-eclosion growth and experience dependent neuropil plasticity

Authors:

Stephen H. Montgomery[1], Richard M. Merrill[2,3], Swidbert R. Ott[4]

Institutional affiliations:

[1] Dept. Genetics, Evolution & Environment, University College London, Gower Street, London, UK, WC1E 6BT

[2] Dept. Zoology, University of Cambridge, Downing Street, Cambridge, UK, CB2 3EJ

[3] Smithsonian Tropical Research Institute, MRC 0580-12, Unit 9100 Box 0948, DPO AA 34002-9998, Panama

[4] Dept. Biology, University of Leicester, Adrian Building, University Road, Leicester, UK, LE1 7RH

Corresponding author: Stephen H. Montgomery: Stephen.Montgomery@cantab.net

Running head: *Anatomy and plasticity of* Heliconius *brains*

Key words: adaptive brain evolution, comparative neuroanatomy, *Heliconius*, Lepidoptera, mushroom bodies, plasticity

Financial support: This research was supported by research fellowships from the Royal Commission of the Exhibition of 1851 and Leverhulme Trust, a Royal Society Research Grant (RG110466) and a British Ecological Society Early Career Project Grant awarded to SHM. RMM was supported by a Junior Research Fellowship from King's College, Cambridge and an Ernyst Mayr Fellowship from STRI. SRO was supported by a University Research Fellowship from the Royal Society, London (UK).

ABSTRACT

Behavioral and sensory adaptations are often based in the differential expansion of brain components. These volumetric differences represent differences in investment, processing capacity and/or connectivity, and can be used to investigate functional and evolutionary relationships between different brain regions. Here, we describe the brain composition of two species of *Heliconius* butterflies, a long-standing study system for investigating ecological adaptation and speciation. We confirm a previous report of striking mushroom body expansion, and explore patterns of post-eclosion growth and experience-dependent plasticity in neural development. This analysis uncovers two phases of post-emergence mushroom body growth comparable to those of foraging hymenoptera, but also identifies plasticity in several other neuropil. An interspecific analysis suggests *Heliconius* may display remarkable levels of investment in mushroom bodies for a Lepidopteran, and indeed rank highly compared to other insects. We also describe patterns of adaptive divergence in the volume of both peripheral and central neuropil within *Heliconius*, and across Lepidoptera, that suggest changes in brain composition plays an important role in ecological adaptation. Our analyses lay the foundation for future comparative and experimental analyses that will establish *Heliconius* as a useful case study in evolutionary neurobiology.

INTRODUCTION

Behavioral adaptations can allow populations to respond to environmental change and to invade new ecological niches. These behavioral changes are largely based in adaptive changes in brain function, which may in turn involve changes in the size and macro-structure of the brain (e.g., Gonda et al., 2009a,b, 2013; Park and Bell, 2010). For example, a clear signature of adaptive, phylogenetic divergence in brain composition in response to ecological variation is seen within many invertebrate and vertebrate species in their sensory neuropil (e.g. Barton et al., 1995; Huber et al., 1997; Gronenberg and Hölldobler, 1999; O'Donnell et al., 2013; Montgomery and Ott, 2015). In this case, nocturnal species, or those occupying low light environments, tend to have larger olfactory neuropil, and smaller visual neuropil (Barton et al., 1995; Montgomery and Ott, 2015).

Beyond the primary sensory regions, ecological selection pressures may have diverse effects on higher brain centers. The complexity of the physical (Capaldi et al., 1999; Safi and Dechmann, 2005; Pollen et al., 2007; Shumway, 2008; Farris and Schulmeister, 2011) or social environment (Barton and Dunbar, 1997; Burish et al., 2004; Lihoreau et al., 2012) have a detectable influence in shaping brain size and structure. For example, in vertebrates, this is clearly manifest in an evolutionary association between the need for spatial memory and the volume of the hippocampus (Clayton and Krebs, 1995; Garamszegi and Eens, 2004). In insects a similar association is found with the mushroom bodies (Farris and Schulmeister, 2011).

Differential expansions of individual brain structures shed light not only on species-specific biology and neuroecology, but more generally on the functional relationships between brain components (Barton and Harvey, 2000; Whiting and Barton, 2003), the relative strength of developmental constraints (Finlay and Darlington, 1995; Barton and Harvey, 2000), and on how very different brains produce seemingly similarly complex behavior (Giurfa and Menzel, 2001; Chittka and Niven, 2009; Farris, 2013).

Given their longstanding role in studies of both adaptation and brain function, the Lepidoptera are perhaps an underutilized group for integrating these fields to investigate evolutionary neurobiology. The Neotropical genus *Heliconius* (Heliconiinae, Nymphalidae) is well known for its diversity of bright warning patterns

that are often involved in Müllerian mimicry, where two or more unpalatable species converge on the same warning-signal to more efficiently advertise their distastefulness to predators (Müller, 1879; Mallet & Barton 1989; Merrill et al 2013). Perhaps as a result these butterflies have been intensively studied, leading to insights into a range of areas including population and community ecology, evolutionary genetics and development, as well as more generally contributing to our understanding of adaptation and speciation (Merrill et al., 2015).

Heliconius display a strong pattern of ecological divergence (Boggs et al., 1981; Estrada and Jiggins, 2002; Jiggins, 2008), and a number of striking behavioral adaptations (Gilbert, 1972, 1975; Mallet, 1986). Chief among these is a dietary adaptation, unique among Lepidoptera; adult pollen feeding (Gilbert, 1972, 1975). With the exception of four species formerly ascribed to the genus *Neruda* (Beltrán et al., 2007; Kozak et al., 2015), all *Heliconius* actively collect and ingest pollen as adults. This provides a rich source of amino acids and permits a greatly extended lifespan of up to six months without reproductive senescence, and shifts the energetic costs of chemical defense to larvae (Gilbert, 1972; Benson, 1972; Ehrlich and Gilbert, 1973; Dunlap-Pianka et al., 1977; Cardoso and Gilbert, 2013). Without access to pollen *Heliconius* suffer a major reduction in longevity and reproductive success (Gilbert, 1972; Dunlap-Pianka et al., 1977; O'Brien et al., 2003).

Adult *Heliconius* collect pollen from a relatively restricted range of mostly Cucurbitaceous plants (Estrada and Jiggins, 2002), which are spatially dispersed and occur at low densities (Gilbert, 1975). Several lines of evidence suggest selection for pollen feeding has shaped *Heliconius* foraging behavior. Individuals inhabit home ranges of typically less than 1 km^2, within which individuals repeatedly utilize a small number of roosting sites that they return to with high fidelity (Turner, 1971; Benson, 1972; Gilbert, 1975; Mallet, 1986; Murawski and Gilbert, 1986; Finkbeiner, 2014). On leaving the roost individuals visit feeding sites with a level of consistency in time and space that strongly suggests 'trap-lining' behavior (Ehrlich and Gilbert, 1973; Gilbert, 1975, 1993; Mallet, 1986), analogous to that observed in foraging bees (Janzen, 1971; Heinrich, 1979). Roosts themselves are located visually (Jones, 1930; Gilbert, 1972; Ehrlich and Gilbert, 1973; Mallet, 1986), and older individuals tend to be more efficient foragers (Boggs et al., 1981; Gilbert, 1993). Together these observations suggest the evolution of pollen feeding in *Heliconius* was facilitated by

an enhanced, visually-orientated 'circadian memory' that utilizes visual landmarks (Gilbert, 1975).

The evolution of this behavior must involve "some elaboration of the nervous system" (Turner, 1981), suggested to lie in the mushroom bodies (Sivinski, 1989). Sivinski (1989) reported that the percentage of the brain occupied by the mushroom body in two individuals of *Heliconius charithonia* was 3–4 times larger than in six other species of butterfly, including two non-pollen feeding Heliconiini. In other insects, mushroom body expansion has been associated with increased demands for higher order information processing, either in relation to social ecology or foraging behavior, both within and between species (Dujardin, 1859; Withers et al., 1993, 2008; Gronenberg et al., 1996; Ehmer and Ron, 1999; Molina and O'Donnell, 2007; Smith et al., 2010; O'Donnell et al., 2013; Gronenberg et al., 1996; Fahrbach et al., 2003; Farris and Roberts, 2005; Farris and Schulmeister, 2011).

Mushroom bodies have a variety of roles in olfactory associative learning, sensory integration, filtering and attention (Zars, 2000; Farris, 2005, 2013; Menzel, 2014). Direct experimental evidence also links mushroom body function with spatial learning and memory in some, but not all, insects (Mizunami et al., 1998; Neuser et al., 2008; Ofstad et al., 2011). Comparisons across species suggest that extreme evolutionary expansion of the mushroom body is commonly associated with changes in foraging behavior that depend on spatial memory or the complexity of sensory information utilized by the species (Farris, 2005, 2013). For example, in Hymenoptera, mushroom body expansion coincides with the origin of parasitoidism (Farris and Schulmeister, 2011), a dietary adaptation that involves place-centered foraging and spatial memory for host location (Rosenheim, 1987; van Nouhuys and Kaartinen, 2008).

Patterns of ontogenetic neuropil plasticity in trap-lining insects, such as the honeybee, *Apis mellifera*, further link foraging behavior and the mushroom bodies (Withers et al., 1993; Durst et al., 1994; Capaldi et al., 1999; Farris et al., 2001). Honeybees show two forms of post-eclosion growth in mushroom body volume; age dependent growth, which occurs regardless of environmental variation, and experience dependent growth which increases with foraging or social experience (Withers et al., 1993; Durst et al., 1994; Fahrbach et al., 1998, 2003; Farris et al., 2001; Maleszka et al., 2009). A similar pattern is found in other Hymenoptera, and there is an intriguing correspondence between the rate and timing of mushroom body

168 growth and the onset of foraging behavior (Gronenberg et al., 1996; Kühn-Bühlmann
169 and Wehner, 2006; Withers et al., 2008; Jones et al., 2013). These combined growth
170 processes involve substantial volumetric changes, typically 20–30% increases from
171 emergence to maturity (Gronenberg et al., 1996; Fahrbach et al., 1998; Jones et al.,
172 2013), which most probably have strong biological and behavioral significance. Age
173 and environmental effects on neuropil growth are also found in some other central and
174 peripheral neuropil (Gronenberg et al., 1996; Jones et al., 2013).Whether *Heliconius*
175 show similar ontogenetic profiles or experience dependent plasticity in mushroom
176 body growth, as might be predicted if they are involved in spatial memory, is not
177 known.

178 Assessing levels of environment dependent neurological plasticity may provide
179 insights into the role behavior may have played during the *Heliconius* radiation, and
180 during speciation in general (Pfennig et al., 2010; Snell-Rood, 2013). Speciation in
181 *Heliconius* is thought to frequently mimetic shifts associated with habitat divergence (
182 Mallet, 1993; Jiggins, 2008). Different mimicry rings represent alternative adaptive
183 peaks, and may be associated with variation in predator communities, interspecific
184 competition, habitat structure and/or light environment (Smiley, 1978; Mallet, 1993;
185 Estrada and Jiggins, 2002; Merrill et al 2013). Consequently, shifts in mimetic
186 resemblance may impose extensive secondary selection for behavioral adaptations.
187 Indeed, several parapatric sister-species occur along habitat gradients (Jiggins et al.,
188 1996; Estrada and Jiggins, 2002; Arias et al., 2008), supporting evidence that different
189 mimicry rings are ecologically separated (Smiley, 1978; Boggs et al., 1981; Estrada
190 and Jiggins, 2002). A potential role for neural plasticity is established in some cases
191 of recent ecological divergence and adaptation (e.g Gonda et al., 2009a; b, 2013; Park
192 and Bell, 2010). Whether habitat-shifts during the early stages of speciation in
193 *Heliconius* are facilitated by behavioral and neurological plasticity is unknown but of
194 considerable interest (Merrill et al., 2015).

195 In the current analysis we begin to investigate these topics. We first revisit
196 *Heliconius* brain composition to confirm Sivinksi's (1989) observation that they are
197 greatly expanded. We then compare brain composition between recently emerged
198 insectary-reared individuals, aged insectary-reared individuals, and wild-caught
199 individuals to address several key questions: i) how big are *Heliconius* mushroom
200 bodies? ii) how does their morphology compare with other trap-line foragers? iii) do
201 they have post-eclosion growth patterns comparable to other trap-line foragers? and

iv) is such environmentally induced plasticity present in, or restricted to, the mushroom bodies? These intra-specific comparisons lay the groundwork for comparative analyses across Heliconiini examining the origin and timing of mushroom body expansion. In the meantime, we compare the relative investment in different neuropil in two species of *Heliconius*, *H. erato* and *H. hecale* to each other, and to other Lepidoptera to explore how selection has shaped overall brain composition.

MATERIALS & METHODS

Animals

We collected individuals of two species of *Heliconius*, *H. hecale melicerta* and *H. erato demophoon*. *H. hecale* is generally found in tall forest throughout central America and the Amazon basin, whilst *H. erato* is a widespread forest edge specialist (Brown, 1981). Wild individuals were collected from Gamboa (9°7.4′ N, 79°42.2′ W, elevation 60 m) and the nearby Soberanía National Park, República de Panamá. At this locality *H. hecale* belongs to the 'tiger pattern' mimicry ring, whilst *H. erato* belongs to the 'postman' mimicry ring which are at least partially segregated by habitat preference (Estrada and Jiggins, 2002). Five males and five females of each species were sampled from the wild. We assume all wild-caught individuals were sexually mature, and that the age range is not biased between species or sexes.

Wild individuals were compared with individuals from first or second-generation insectary-reared stock populations, descended from wild caught parents from the same sampling localities. Stock populations were kept in controlled conditions in cages (approximately 1 × 2 × 2 m) of mixed sex at roughly equal densities. Cages were housed at the *Heliconius* insectaries at the Smithsonian Tropical Research Institute's (STRI) facility in Gamboa (see: www.heliconius.org/resources/research-facility). Stocks had access to their preferred host plant (*Passiflora biflora* and *P. vitifolia* respectively for *H. erato* and *H. hecale*), a pollen source (*Psychotria elata*) and feeders containing c. 20% sugar solution with an additional bee-pollen supplement to ensure there was a pollen excess. Larvae were allowed to feed naturally on the host plant.

After emergence from the pupae insectary-reared individuals were collected for two age groups, a recently emerged 'young' group (1–3 days post emergence) and an 'old' group (2–3 weeks post emergence). *Heliconius* are generally considered to undergo a "callow" period of general inactivity immediately after emergence that lasts about 5 days, during which flight behavior is weak and males are sexually inactive (Mallet, 1980). These age groups therefore represent behaviorally immature and mature individuals. In *Bombus impatiens*, which has a comparable lifespan to *Heliconius* (Plath, 1934; Benson, 1972; Ehrlich and Gilbert, 1973), age-related growth plateaus after c. 10 days (Jones et al., 2013). If *Heliconius* have a comparable developmental trajectory we would expect growth to have reached a plateau in the old group. For *H. hecale* 5 males and 5 females were sampled for both age groups, in *H. erato* 4 males and 6 females were sampled for the 'young' group and 5 males and 4 females were sampled for the 'old' group. For samples where it was possible to measure the exact time of emergence, there is no significant difference between *H. hecale* and *H. erato* in age structure of the old (*H. erato*: mean = 22.6 days, SD = 8.6; *H. hecale*: mean = 26.4 days, SD = 5.5; t_{13} = -0.899, p = 0.385) or young (*H. erato*: mean = 1.7 days, SD = 0.8; *H. hecale*: mean = 1.3 days, SD = 1.1; t_{17} = 0.829, p = 0.419) insectary-reared groups.

We took three body size measurements for each individual: body mass, weighted to 0.01 g using a OHAUS "Gold Pocket" pocket balance (model YA102); and body length and wingspan, measured using FreeLOGIX 6 inch digital calipers. Wings were kept as voucher specimens in glassine envelopes. Samples were collected and exported under permits SEX/A-3-12 and SE/A-7-13 obtained from the Autoridad Nacional del Ambiente, República de Panamá in conjunction with STRI.

Antibodies and sera for neuropil staining

We used indirect immunofluorescence staining against synapsin to reveal the neuropil structure of the brain under a confocal microscope (Ott, 2008). This technique exploits the abundant expression of synapsin, a vesicle-associated protein, at presynaptic sites. Monoclonal mouse anti-synapsin antibody 3C11 (anti-SYNORF1; (Klagges et al., 1996) was obtained from the Developmental Studies Hybridoma Bank (DSHB), University of Iowa, Department of Biological Sciences, Iowa City, IA 52242, USA (RRID: AB_2315424). The 3C11 antibody was raised against a bacterially expressed fusion protein generated by adding a glutathione S-transferase

(GST)-tag to a cDNA comprising most of the 5′ open reading frame 1 of the *Drosophila melanogaster* synapsin gene (*Syn,* CG3985). The binding specificity of this antibody was characterised in *D. melanogaster* (Klagges et al., 1996). The epitope was later narrowed down to within LFGGMEVCGL in the C domain (Hofbauer et al., 2009). Bioinformatic analysis has confirmed the presence of this motif in Lepidopteran genomes, and demonstrated that it is highly conserved across Lepidoptera (Montgomery and Ott, 2015). 3C11 immunostaining has been used as an anatomical marker of synaptic neuropil in a wide range of arthropod species including several Lepidoptera: *Danaus plexippus* (Heinze and Reppert, 2012), *Godyris zavaleta* (Montgomery and Ott, 2015) *Heliothis virescens* (Kvello et al., 2009) and *Manduca sexta* (El Jundi et al., 2009b). The staining pattern obtained with 3C11 in the present analysis is similar to other Lepidoptera. Cy2-conjugated affinity-purified polyclonal goat anti-mouse IgG (H+L) antibody (Jackson ImmunoResearch Laboratories, West Grove, PA) was obtained from Stratech Scientific Ltd., Newmarket, Suffolk, UK (Jackson ImmunoResearch Cat No. 115-225-146, RRID: AB_2307343).

Immunocytochemistry

Brains were fixed and stained following a published protocol (Ott, 2008) previously applied to a range of invertebrates including the Monarch butterfly, *D. plexippus* (Heinze and Reppert, 2012), and the Zavaleta Glasswing, *G.* (Montgomery and Ott, 2015). The protocol was divided into two stages, the first of which was performed at the STRI Gamboa Field Station. Briefly, the brain was exposed under HEPES-buffered saline (HBS; 150 mM NaCl; 5 mM KCl; 5 mM $CaCl_2$; 25 mM sucrose; 10 mM HEPES; pH 7.4) and fixed in situ for 16–20 hours at room temperature (RT) in zinc-formaldehyde solution (ZnFA; 0.25% (18.4 mM) $ZnCl_2$; 0.788% (135 mM) NaCl; 1.2% (35 mM) sucrose; 1% formaldehyde) under agitation. Fixation with ZnFA affords considerably better antibody penetration, staining intensity and preservation of morphology than conventional (para)formaldehyde fixation (Ott, 2008; Heinze and Reppert, 2012). The brain was subsequently dissected out, under HBS, by removing the eye cuticle in slices before gently plucking away the main body of the ommatidia and the basement membrane. After removing any surrounding material, the brain was lifted from the head capsule, washed 3 × in HBS and placed into 80% methanol/20% DMSO for a minimum of 2 hours under agitation. The brain was then transferred to

100% methanol and stored at RT. After transportation back to the UK samples were stored at -20˚C.

In the second stage of the protocol, performed in laboratory conditions in the UK, the samples were brought to RT and rehydrated in a decreasing methanol series (90%, 70%, 50%, 30%, 0% in 0.1 M Tris buffer, pH 7.4, 10 minutes each). Normal goat serum (NGS; New England BioLabs, Hitchin, Hertfordshire, UK) and antibodies were diluted in 0.1 M phosphate-buffered saline (PBS; pH 7.4) containing 1% DMSO and 0.005% NaN_3 (PBSd). Non-specific antibody binding was blocked by pre-incubation in 5% NGS (PBSd-NGS) for 2 hours at RT. Antibody 3C11 was then applied at a 1:30 dilution in PBSd-NGS for 3.5 days at 4˚C under agitation. The brains were rinsed in PBSd for 3 × 2 hours before applying the Cy2-conjugated anti-mouse antibody 1:100 in PBSd-NGS for 2.5 days at 4˚C under agitation. This was followed by a series of increasing concentrations (1%, 2%, 4% for 2 hours each, 8%, 15%, 30%, 50%, 60%, 70% and 80% for 1 hour each) of glycerol in 0.1 M Tris buffer with DMSO to 1%. The brains were then passed in a drop of 80% glycerol directly into 100% ethanol and agitated for 30 minutes; the ethanol was changed three times with 30-minute incubations. Finally, to clear the tissue, the ethanol was underlain with methyl salicylate, the brain was allowed to sink, before the methyl salicylate was refreshed twice with 30 minute incubations.

Confocal imaging

Samples were mounted in fresh methyl salicylate between two round cover slips separated by a thin metal washer (UK size M8 or M10). All imaging was performed on a confocal laser-scanning microscope (Leica TCS SP8, Leica Microsystem, Mannheim, Germany) at the University College London Imaging Facility, using a 10× dry objective lens with a numerical aperture of 0.4 (Leica Material No. 11506511, Leica Microsystem, Mannheim, Germany). For each individual brain we captured a series of overlapping stacks using a mechanical *z*-step of 2 µm with an *x*-*y* resolution of 512 × 512 pixels. Imaging the whole brain required 3×2 stacks in the *x*-*y* dimensions with an overlap of 20%. Tiled stacks were automatically merged in Leica Applications Suite Advanced Fluorescence software. Each brain was scanned from the posterior and anterior side to span the full *z*-dimension of the brain. These two image stacks were subsequently merged in Amira 3D analysis software 5.5 (FEI

Visualization Sciences Group), using a custom module 'Advanced Merge' which aligns images using affine registration and subsequently merges to produce the combined stacks. We manually optimized the re-sampling procedure from anterior and posterior stacks for each individual. Finally, to correct for the artifactually shortened *z*-dimension associated with the 10× air objective, a correction factor of 1.52 was applied to the voxel size in the *z*-dimension (Heinze and Reppert, 2012a; Montgomery and Ott, 2015). Images presented in the figures to illustrate key morphological details were captured separately as single confocal sections with an *x-y* resolution of 1024 × 1024 pixels.

Neuropil segmentations and volumetric reconstructions

Neuropils were reconstructed from the confocal image stacks in Amira 5.5. We assigned image regions to anatomical structures in the Amira *labelfield* module by defining outlines based on the brightness of the synapsin immunofluorescence. This process segments the image into regions that are assigned to each particular structure, and regions that are not. Within each stack, every forth or fifth image was manually segmented using the outline or magic-wand tool. The segmentation was then interpolated in the *z*-dimension across all images that contain the neuropil of interest before being fine-edited and smoothed in all three dimensions. The *measure statistics* module was used to determine volumes (in μm^3) for each neuropil. 3D polygonal surface models of the neuropils were constructed from the smoothed labelfield outlines using the *SurfaceGen* module. The color code used for the neuropils in the 3D models is consistent with previous neuroanatomical studies of invertebrate brains (Brandt et al., 2005; Kurylas et al., 2008; El Jundi et al., 2009a, b; Dreyer et al., 2010; Heinze and Reppert, 2012; Montgomery and Ott, 2015).

The whole-brain composite stacks were used to reconstruct and measure six paired neuropils in the optic lobes, and seven paired and two unpaired neuropils in the midbrain. All paired neuropils were measured on both sides of the brain in wild-caught individuals to permit tests of asymmetry, yielding two paired measurements per brain (*i.e.,* $N = 10 \times 2$) for each structure. We found no evidence of volumetric asymmetry for either species ($p > 0.05$ for each neuropil in a paired t-tests) and therefore summed the volumes of paired neuropil to calculate the total volume of that structure. In insectary-reared individuals we therefore subsequently measured the

volume of paired neuropil from one hemisphere, chosen at random, and multiplied the measured volume by two to obtain an estimate of total volume of that neuropil. Finally, we measured the total neuropil volume of the midbrain to permit statistical analyses that control for allometric differences. In keeping with the earlier Lepidopteran literature, we use the term 'midbrain' for the fused central mass that comprises of the protocerebral neuromere excluding the optic lobes, the deuto- and tritocerebral neuromeres, and the sub-esophageal neuromeres. For the following statistical analyses we analyzed the central body as a single structure, and summed the volumes of the mushroom body lobes and peduncles as the boundary between these structures was not always clear.

Intraspecific statistical analyses

In all statistical analyses continuous variables were $\log_{10}$-transformed to meet assumptions of normality. Unpaired two-tailed two-sample *t*-tests were used to test for volumetric differences between sexes or groups. We found no robust evidence of sexual dimorphism in neuropil volume of wild caught individuals that could not be explained by allometric scaling and therefore combined male and female data. However, we note that our sample size for each sex is unlikely to be sufficient to provide conclusive support either for or against sexual dimorphism.

Our analyses focused on two intra-specific comparisons: i) we compared 'young' and 'old' insectary-reared individuals and interpret significant differences as evidence for post-eclosion growth or delayed maturation; and ii) we compared wild-caught individuals with 'old' insectary-reared individuals and interpret significant differences as evidence for environmentally induced, experience dependent plasticity. These comparisons were made by estimating the allometric relationship with a measure of overall brain size for each neuropil. The standard allometric scaling relationship can be modeled as $\log(y) = \beta[\log(x)] + \alpha$. We used standard major axis regressions in the SMATR 3 package (Warton et al., 2012) to test for significant shifts in the allometric scaling parameter (β) or the y-intercept (α). To permit comparisons between neuropil, a consistent independent variable was used throughout the analyses that accounts for allometric scaling with total brain size. This was the total volume of the midbrain minus the combined volume of all segmented neuropil in the midbrain, referred to as 'rest of midbrain' (rMid).

Significant differences in β suggest the proportional increase in the dependent variable with size differs between groups, i.e. the slopes are significantly different. The *slope.com* function in SMATR calculates a likelihood ratio statistic for the absence of a common slope, χ^2 distributed with one degree of freedom. Where we identified no heterogeneity in the allometric scaling parameter (β) we performed two further tests. First, we tested for significant differences in α that suggest discrete 'grade-shifts' in the relationship between two variables. The *elev.com* function in SMATR calculates a Wald statistic for the absence of shifts along the y-axis, χ^2 distributed with one degree of freedom. Second, we tested for major axis-shifts along a common slope. This is indicative of co-ordinated changes in the size of the dependent and independent variable between groups. The *shift.com* function in SMATR calculates a Wald statistic for the absence of a shift along a common axis, χ^2 distributed with one degree of freedom. For this test, when significant, we also report the fitted axis (FA) mean that describes the mean position of the group on the common fitted axis. For all statistically significant tests we also present the effect size, measured by the correlation coefficient (r). Effect sizes of $0.1<r<0.3$ are interpreted as 'small' effects, $0.3<r<0.5$ 'medium' effects, and $r<0.5$ 'large' effects (Cohen, 1988).

Patterns of brain:body allometry were explored in a similar manner, using total neuropil volume as the dependent variable (summed volumes of all neuropil in the optic lobes plus the total midbrain volume), and comparing the results obtained using alternative body size measurements as the independent variable. Body mass varies with body condition and reproductive state, we therefore anticipated that body length may be a more reliable way of assessing the allometric relationship between brain and body size in wild caught individuals.

We complemented these analyses with a multivariate analysis of all segmented neuropil volumes and the unsegmented midbrain volume using Discrimant Function Analysis (DFA) to test how reliably individuals can be assigned to their respective groups on the basis of their volumetric differences in neuropil. In this analysis, as well as providing a percentage of correctly assigned individuals, Wilks' lambda provides a measure of the proportion of total variance not explained by group differences, and the χ^2 statistic provides a test for significant group differences. All statistical analyses were performed in R (R Development Core Team, 2008), using the

standard *stats* and *smatr* package, except for the DFA, which was performed in SPSS v. 22 for OS X (SPSS Inc., Chicago, IL)

Interspecific statistical analyses

An examination of allometric scaling was also applied to interspecific analyses between *H. hecale* and *H. erato* to test for species differences in brain composition. We compared both wild-caught and 'old' insectary-reared individuals. Where significant species differences are found in wild caught individuals but not 'old' insectary-reared individuals we interpret this as evidence of species-dependent environmental effects, perhaps associated with differences in habitat or light-environment preference. Where significant species differences are found for both comparisons we interpret this as evidence of heritable differences in brain development.

We collected published data for neuropil volumes of four other Lepidoptera; the Monarch butterfly (*D. plexippus*; Heinze and Reppert, 2012), the Zavaleta Glass wing (*Godyris zavaleta*; Montgomery and Ott, 2015), the Giant Sphinx moth (*Manduca sexta*; El Jundi et al., 2009b) and the Tobacco Budworm moth (*Heliothis virescens*; Kvello et al., 2009). Data were available for eight neuropils across all four species. We calculated the relative investment in each neuropil by comparing its volume to the total neuropil volume of either the whole brain (excluding the lamina, which was not measure in *Heliothis virescens*), or of only the midbrain. Relative size was measured by calculating the residuals from a phylogenetically-corrected least squares (PGLS) linear regression between each structure and the rest of the brain performed in BayesContinous in BayesTraits (freely available from www.evolution.rdg.ac.uk; Pagel, 1999). For this analysis, a phylogeny of the six species was created using data on two loci, *COI* and *EF1a* (GenBank Accession IDs, *COI*: EU069042.1, GU365908.1, JQ569251.1, JN798958.1, JQ539220.1, HM416492.1; *EF1a*: EU069147.1, DQ157894.1, U20135.1, KC893204.1, AY748017.1, AY748000.1). The data were aligned and concatenated using MUSCLE (Edgar, 2004), before constructing a maximum likelihood tree in MEGA v.5 (Tamura et al., 2011). Differences in brain architecture across species were visualised by multivariate Principal Component Analysis of these data, and visualized as biplots (Greenacre, 2010) in R package *ggbiplot* (V.Q. Vu, https://github.com/vqv/ggbiplot).

Finally, we extended our phylogenetic analysis across insects using a similar approach. We restricted this analysis to volumetric data collected with similar methodology (Rein et al., 2002; Brandt et al., 2005; Kurylas et al., 2008; Dreyer et al., 2010; Ott and Rogers, 2010; Wei et al., 2010) as it is not known how comparable data collected with alternative fixing, staining and imaging methods are. The phylogenetic relationship of these insects was taken from Trautwein et al. (2012).

RESULTS

General layout of the *Heliconius* brain

In general, the overall layout and morphology of the *Heliconius* brain (Fig. 1) is similar to that of other Lepidoptera (El Jundi et al., 2009; Kvello et al., 2009; Heinze and Reppert, 2012a; Montgomery and Ott, 2015). The midbrain forms a single medial mass, containing the supra-esophageal ganglion to which the sub-esophageal ganglion is fused. Synapsin immunostaining effectively labeled regions of synaptic neuropil, with minimal fluorescence in fiber tracts and cell bodies, permitting segmentation of six paired neuropils in the optic lobes, and eight paired and two unpaired neuropils in the midbrain. Together with the rest of the midbrain (rMid), which lacks distinct internal boundaries, we measured the volumes of these neuropils in 59 individuals across both species (Table 1). In the following we briefly describe the main anatomical features of the sensory neuropils, the central complex and the mushroom bodies in wild individuals. We then present the results of intra-specific comparisons between age groups, between wild and insectary-reared individuals, before moving to an analysis of inter-specific comparisons between *H. hecale* and *H. erato*, and across a wider taxonomic scale.

Sensory neuropil

As expected for a strongly visual, diurnal butterfly, the optic lobes (OL; Fig. 2A–H) account for a large proportion of total brain volume (approximately 64%). As is the case in both *D. plexippus* and *G. zavaleta* the lamina (La), two-layered medulla (Me) (Fig. 2E), accessory medulla (aMe), lobula (Lob) and lobula plate (Lop) are well defined and positioned in the OL as nested structures, running lateral to medial (Fig. 2A). The La has a distinct, brightly stained inner rim (iRim; Fig. 2E), a feature

499 common to all diurnal butterflies analyzed thus far (Heinze and Reppert, 2012;
500 Montgomery and Ott, 2015). In common with *D. plexippus* we identify a thin strip of
501 irregularly shaped neuropil running ventrally from the aME to the Me (Fig. 2G–H).
502 We also identify a sixth neuropil in the OL that we believe to be homologous
503 to the optic glomerulus (OG; Fig. 2B,F) identified in *D. plexippus* (Heinze and
504 Reppert, 2012), which is absent in other Lepidopteran brains described to date and
505 was postulated to be Monarch-specific. As in *D. plexippus* this neuropil is a multi-
506 lobed, irregularly shaped structure positioned to the medial margin of the Lob with
507 which it appears to be connected. In *Heliconius* the OG is not as extended in the
508 anterior margin as *D. plexippus* and is subsequently confined to the OL, without
509 protrusion into the optic stalk or midbrain (Fig. 2A,B,F). The position of the OG in
510 *Heliconius* is also similar to that of a much smaller neuropil observed in *G. zavaleta*
511 (Montgomery and Ott, 2015). We suggest these structures may be homologous but
512 differentially expanded.
513 The midbrain contains two further neuropils with primary functions in
514 processing sensory information; the anterior optic tubercule (AOTu), a visual center,
515 and the antennal lobe (AL), the primary olfactory neuropil. We can identify all four
516 components of the AOTu previously described in *D. plexippus* and *G. zavaleta*
517 butterflies (Heinze and Reppert, 2012; Montgomery and Ott, 2015); the small, closely
518 clustered nodular unit (NU), strap (SP) and lower unit (LU), and the much larger
519 upper unit (UU) (Fig. 2C). As in other butterflies, the UU is expanded compared with
520 nocturnal moths (El Jundi et al., 2009; Kvello et al., 2009). The proportion of total
521 neuropil comprised of the AOTu is, however, larger in *D. plexippus* (0.736%) than
522 *Heliconius* (0.400% in *H. hecale* and 0.368% in *H. erato*).
523 The AL are innervated by the antennal nerves and comprise the central fibrous
524 neuropil (CFN) around which small, round glomeruli are arranged (Figure 3A,B). In
525 *Heliconius* the AL comprises 2% of the total brain neuropil volume, and contains
526 approximately 68 glomeruli (estimated in one individual of each sex: *H. erato* ♂ = 69,
527 ♀ = 68; *H. hecale* ♂ = 68, ♀ = 67). This is similar to estimates for other Lepidoptera,
528 which generally range between 60 and 70 (Boeckh and Boeckh, 1979; Rospars, 1983;
529 Berg et al., 2002; Huetteroth and Schachtner, 2005; Masante-Roca et al., 2005; Skiri
530 et al., 2005; Kazawa et al., 2009; Heinze and Reppert, 2012; Carlsson et al., 2013;
531 Montgomery and Ott, 2015), and the number of olfactory receptor genes (70)
532 identified in the *H. melpomene* genome (Dasmahapatra et al., 2012). We observe no

533 expanded macro-glomeruli or obvious candidates for sexual dimorphic glomeruli
534 suggesting an absence of any MGC-like structure in *Heliconius*. This is in keeping
535 with all diurnal butterflies described to date (Rospars, 1983; Heinze and Reppert,
536 2012; Carlsson et al., 2013), with the exception of the more olfactorily orientated *G.*
537 *zavaleta* in which the AL is 5% of total neuropil volume and a sexually dimorphic
538 MGC is observed (Montgomery and Ott, 2015).

539 We took advantage of comparable datasets for *H. erato, H. hecale* and *G.*
540 *zavaleta* to further investigate the significance of changes in AL size by testing
541 whether changes in relative AL volume are due to an increased volume of glomeruli
542 or CFN. The former would reflect heightened olfactory sensitivity, as larger glomeruli
543 receive more projections from sensory neurons, while the latter may indicate changes
544 in the number or complexity of local interneurons. We find evidence for a grade-shift
545 in the allometric relationship between total glomerular volume and midbrain volume
546 when *G. zavaleta* is compared to either *H. erato* (Wald $\chi^2 = 10.709$, $p = 0.001$) or *H.*
547 *hecale* (Wald $\chi^2 = 9.139$, $p = 0.003$) (Fig. 3C, circles). We also identify a grade-shift
548 between CFN volume and midbrain volume in *G. zavaleta* over *H. erato* (Wald $\chi2 =$
549 30.282, $p < 0.001$) and *H. hecale* (Wald $\chi^2 = 26.638$, $p < 0.001$) (Fig. 3C, triangles).
550 Hence, AL expansion in *G. zavaleta* is due to changes in both CFN and glomerular
551 volume. However, when comparing CFN and glomerular volume directly against one
552 another we again find a significant grade-shift in *G. zavaleta* over *H. erato* (Wald $\chi^2 =$
553 19.680, $p < 0.001$) and over *H. hecale* (Wald $\chi^2 = 31.663$, $p < 0.001$) demonstrating
554 greater CFN volume, relative to glomerular volume, in *G. zavaleta* (Fig. 3D). This
555 suggests variation in Lepidopteran AL size may be largely explained by changes in
556 the complexity of olfactory processing, which may in turn explain the consistency in
557 glomerular number across species with contrasting diel patterns (see above).
558
559 **Central complex**
560 The central complex is a multimodal integration center linked to a range of functions
561 from locomotor control to memory (Pfeiffer and Homberg, 2014). Within the
562 limitations of the current analysis, the anatomy of the *Heliconius* central complex
563 shows strong conservation with *D. plexippus* and *G. zavaleta* (Heinze and Reppert,
564 2012; Montgomery and Ott, 2015). The central body (CB) is positioned along the
565 midline of the central brain and is formed of two neuropils, the upper (CBU) and
566 lower (CBL) divisions, which are associated with small paired neuropils, the noduli

(No), located ventrally to the CB (Fig. 4A–D,G). Two further paired neuropils, the protocerebral bridge (PB; Fig. 4A,E) and posterior optic tubercles (POTu; Fig. 4A,F), are positioned towards the posterior margin of the brain.

Mushroom bodies

The most striking aspect of *Heliconius* brain morphology are the hugely expanded mushroom bodies, previously noted by Sivinski (1989). These neuropils span the depth of the brain along the anterior-posterior axis (Fig. 5A–K; Fig. 6A,A'). On the anterior side, the mushroom body lobes (MB-lo) lie above the AL. As in *D. plexippus* (Heinze and Reppert, 2012a) the distinct lobe structure observed in moths (El Jundi et al., 2009; Kvello et al., 2009) is lost, possibly due to extensive expansion. The only identifiable feature is a lobe curving round the medial margin, likely to be part of the vertical lobe (Fig. 5D,F). The MB-lo merges with a long cylindrical neuropil, the pedunculus (MB-pe) that extends to the posterior midbrain and is comprised of several twisted layers of neuropil. The boundary between the MB-lo and MB-pe is not distinct. The combined volume of the MBlo+pe accounts for 12.2% of total midbrain volume in *H. hecale* and 14.6% of total midbrain volume in *H. erato*, at least twice that reported for other Lepidoptera (Sjöholm et al., 2005; El Jundi et al., 2009; Kvello et al., 2009; Heinze and Reppert, 2012a; Montgomery and Ott, 2015). At the posterior end, the MB-pe splits into two roots that are encircled by the mushroom body calyx (MB-ca; Fig. 5A,H,K). A Y-tract runs parallel to the MB-pe from the posterior boundary of the MB-lo to the junction between the MB-pe and MB-ca. The Y-tract ventral loblets seen in other Lepidoptera (El Jundi et al., 2009; Kvello et al., 2009) are not distinct, presumably having merged with the MB-lo (Fig. 5A,J,N).

The MB-ca is a deeply cupped, un-fused, double-lobe structure (Fig. 5A,C). Two concentric zones can be identified (Fig. 5E), though the boundary is not distinct throughout the depth of the neuropil. The MB-ca comprises 20.7% and 23.9% of total midbrain volume in *H. hecale* and *H. erato* respectively, at least three times greater than reported in other Lepidoptera (Sjöholm et al., 2005; El Jundi et al., 2009; Kvello et al., 2009; Heinze and Reppert, 2012a; Montgomery and Ott, 2015). In some individuals the MB-ca is so large that it protrudes into the OL resulting in a distortion of shape caused by constriction around the optic stalk (Fig. 5H). We also observe some degree of pitting in the posterior surface of the MB-ca (Fig. 5I). This pitting is

related to radially arranged columnar domains that are apparent within the calycal neuropil (Fig. 5J,K,M)

Below the junction between MB-pe and MB-ca is a brightly stained globular neuropil with a poorly defined anterior margin (Fig. 5M). It is possible this is an accessory calyx, which has a sporadic phylogenetic distribution across Lepidoptera and other insects (Farris, 2005). However, accessory calyces are generally positioned closely to the MB-pe/MB-ca, as is observed in *D. plexippus* (Heinze and Reppert, 2012). This neuropil also lacks the 'spotty' appearance of the accessory calyx in *D. plexippus* (Heinze and Reppert, 2012). We therefore do not believe this is an accessory calyx. Similar 'satellite' neuropils that are near, but not directly linked to the mushroom bodies are observed in other insects, for example *Neuroptera* (Farris, 2005). One potentially interesting observation is that this neuropil lies in a position roughly equivalent to the anterior end of the OG in *D. plexippus* (Heinze and Reppert, 2012). Although generally unclear, in some individuals it is possible to follow a narrow, weakly stained fiber tract from the medial margin of the Lob/OG to this position, via an area of relatively intense staining in the optic stalk (Fig. 5L). It is possible this neuropil is functionally connected to the OG, and that OG expansion along the anterior margin in *D. plexippus* occurred along the path of this pre-existing connection, resulting in a single, elongated neuropil. In other insects the MB-pe also receives afferent innervation from regions of the protocerebrum other than the MB-ca (Schürmann, 1970; Li and Strausfeld, 1997, 1999). A pronounced fiber tract emanating from the AOTu UU clearly runs against the dorsal boundary of the MB-pe (Figure 5O), but whether or not there is a functional connection, that might suggest the integration of processed visual information with the MB-pe/lo, is unclear.

Brain:body allometry

The relationship between total neuropil and body mass is not significant at $p > 0.05$ for either wild *H. hecale* (log-log SMA regression, $p = 0.055$) or wild *H. erato* ($p = 0.863$). However, as expected body mass is more variable than either body length or wingspan (*H. hecale,* relative SD of body mass = 15.32%, body length = 10.43%, wingspan = 9.08%; *H. erato,* relative SD of body mass = 19.00%, body length = 5.98%, wingspan = 4.59%), most likely due to differences in feeding and reproductive state. When either body length or wingspan is used as the measure of body size a significant association is recovered both in *H. hecale* (body length $p = 0.020$,

wingspan $p = 0.019$) and in *H. erato* (body length $p = 0.011$, wingspan $p = 0.010$). We subsequently used body length to compare the relationships between total neuropil volume and body size between groups.

We identified a significant grade-shift, between the young and old groups of both *H. erato* and *H. hecale*, in the scaling relationship between total neuropil and body length (*H. hecale:* Wald $\chi^2 = 5.780$, $p = 0.016$; *H. erato:* Wald $\chi^2 = 10.124$, $p = 0.001$). However, there is no significant difference in body length for either species between old and young insectary-reared individuals (*H. hecale* $t_{18} = -0.918$, $p = 0.371$; *H. erato* $t_{17} = 0.581$, $p = 0.568$) suggesting the effect is primarily driven by an increase in neuropil volume. Indeed, there is a significant difference in total neuropil volume between the young and old insectary-reared age groups in *H. erato* ($t_{17} = 5.153$, $p < 0.001$, $r = 0.708$; Fig. 7A). This difference is observed for both total midbrain volume ($t_{17} = 4.192$, $p = 0.001$, $r = 0.713$) and total OL volume ($t_{17} = 5.076$, $p < 0.001$, $r = 0.776$; Fig. 7A). In *H. hecale* a significant difference between young and old individuals is only observed for midbrain volume ($t_{18} = 3.054$, $p = 0.007$, $r = 0.595$), but not OL volume ($t_{18} = 0.280$, $p = 0.783$) or total neuropil volume ($t_{18} = 1.082$, $p = 0.293$; Fig. 7D).

In *H. hecale*, the total neuropil is also 40% larger in wild caught individuals than in old insectary-reared individuals ($t_{17} = 2.553$, $p = 0.020$, $r = 0.526$) driven by a significant difference in midbrain volume ($t_{17} = 3.658$, $p = 0.002$, $r = 0.664$), but not OL volume ($t_{18} = 1.728$, $p = 0.101$; Fig. 7D). We also do not observe a similar difference in body length between wild and old insectary-reared individuals (*H. hecale* $t_{18} = 0.983$, $p = 0.436$). Although this does not result is a grade-shift between wild and old insectary-reared individuals for body length and total neuropil volume (Wald $\chi^2 = 2.058$, $p = 0.151$), we do observe a grade-shift when midbrain is analysed separately (Wald $\chi^2 = 4.725$, $p = 0.030$) No significant volume or size differences are found between wild and old insectary-reared individuals in *H. erato* (total neuropil: $t_{17} = -0.432$, $p = 0.671$; midbrain: $t_{17} = -0.732$, $p = 0.474$; OL: $t_{17} = -0.123$, $p = 0.904$; body length: $t_{17} = 1.009$, $p = 0.327$; Fig. 7A).

Post-eclosion growth in the volume of individual neuropil regions

Evidence of significant age-effects on volume was uncovered for many neuropil regions in both species, indicating an important role for post-eclosion brain

maturation. In *H. erato* volumetric differences between the age groups are widespread, with only the OG failing to show a significant expansion in old individuals (Table 2A). There is some evidence for age-related differences in the allometric scaling coefficients for aMe and PB, and for grade-shifts in OG and POTu, but these are weak relative to the strong major axis shifts observed for all segmented neuropils (Table 2A). The largest shifts are observed for the POTu (difference in fitted-axis (FA) mean = 0.604), aME (difference in FA mean 0.536), MB-ca (difference in FA mean = 0.496) and MB-lo+ped (difference in FA mean = 0.393; Fig. 6A-C).

In *H. hecale* old insectary-reared individuals have significantly larger absolute midbrain volumes ($t_{18} = 3.054$, $p = 0.007$, $r = 0.584$) but not OL volumes ($t_{18} = 1.728$, $p = 0.101$). However, not all segmented midbrain neuropil show the same expansion; the rMid, components of the mushroom body complex, central complex and AL are all significantly larger in old individuals, but the AOTu, POTu and all optic lobe neuropil are not (Table 2B). Neuropil expansion appears to occur in a co-ordinated manner, maintaining the allometric relationship between the segmented neuropil and rMid (Table 2B). The only exceptions are the La, Me and OG, which show significant grade-shifts resulting in a reduced volume of these neuropil relative to rMid volume in old individuals. All other segmented neuropil show major-axis shifts along a common slope towards higher values in old individuals (Table 2B). The largest shifts are observed for the MB-ca (difference in fitted-axis mean = 0.279) and MB-lo+ped (difference in fixed axis mean = 0.250; Fig. 6A'–C').

Experience-dependent plasticity in neuropil volume

The strong contribution of post-emergence growth to brain maturation in *Heliconius* provides a potential window during which the environment could influence the size of different neuropil. We compared wild and old insectary-reared individuals to test for the presence of such environment-dependent neural plasticity. A clear signature of environmentally induced volumetric differences is found in both species, but the pattern differs between them.

In *H. erato* wild individuals do not have significantly larger absolute neuropil volumes for any measured trait (Table 3A). However, several neuropils show evidence of differences in allometric scaling or grade-shifts between wild and old insectary-reared individuals. The neuropil affected by altered scaling coefficients (β)

include the MB-ca, the Lop, and the PB, all of which result shallower scaling realtionships with rMid volume in wild caught individuals (Table 3A; Figure 7B,C). The MB-lo+ped is the only neuropil to show an unambiguous grade-shift whilst maintaining a common slope, and also shows a major axis shift (difference in FA mean = 0.250; Fig. 6B).

In *H. hecale* wild individuals have significantly larger total midbrains (t_{18} = 3.658, p = 0.002). The only segmented neuropil to reflect this difference are the MB-ca and MB-lo+ped (Table 3B; Fig. 6A'-C'), while the rMid is also larger in wild individuals (t_{18} = 3.417, p = 0.003). For example, the average MB-ca volume of old insectary-reared individuals is only 68.3% of the average wild MB-ca volume, for the young insectary-reared individuals it is 49.3% (Figure 6A',C'). For MB-lo+pe these figures are 76.9% and 58.7% respectively (Figure 6A',B'). For comparison, in *H. erato* the average MB-ca volume of old insectary-reared individuals is 96.2% of the average wild MB-ca volume, for the young insectary-reared individuals it is 59.7% (Fig. 6A–C). For MB-lo+pe these figures are 96.9% and 63.9% respectively (Fig. 6A–C).

The only neuropil in the optic lobes to differ significantly volume in *H. hecale* is the Me. The allometric relationship between neuropil volumes and rMid differs for all neuropil either in the allometric scaling coefficient or the intercept, except for the mushroom body components and aMe.(Table 3A; Figure 7E,F). However, for aME this pattern is caused by a lack of allometric scaling in insectary-reared individuals (SMA p = 0.552). The mushroom bodies show evidence of a major axis shift along a common slope (difference in FA mean MB-ca = 0.355, MB-lo+ped = 0.299). Given all grade-shifts result in smaller neuropil volumes relative to rMid (Fig. 7E,F) volume we interpret this as indicating the rMid and mushroom bodies show coordinated environment-dependent increases in volume whilst other neuropil volumes remain largely constant, but with subsequently altered allometric relationships with rMid.

These results highlight potential differences in the maturation and plasticity of brain size and structure between *H. hecale* and *H. erato*. Most notably the rMid appears to have greater amounts of environment-dependent growth in *H. hecale* which results in altered scaling relationships with other neuropil. In *H. hecale* this is accompanied by coordinated expansion of the mushroom body components, which, in volumetric terms is less pronounced in *H. erato*. Instead, the mushroom bodies, along

735 with PB and LoP, are relatively larger in wild *H. erato* due to a grade-shift in the
736 scaling relationship with rMid.
737
738 **Divergence in brain composition between *H. hecale* and *H. erato***
739 *H. hecale* is significantly larger than *H. erato* for all body size measurements (wild
740 caught: body mass $t_{17} = 7.262$, $p < 0.001$; body length $t_{17} = 5.442$, $p < 0.001$; wingspan
741 $t_{17} = 6.071$, $p < 0.001$). *H. hecale* also have larger midbrain ($t_{17} = 2.713$, $p = 0.014$, $r =$
742 *0.539*) and OL volumes ($t_{17} = 2.866$, $p = 0.010$, $d = 1.351$). This difference does not,
743 however, match the body size difference, resulting in a grade-shift in the allometric
744 relationship between body length and total neuropil volume between the species
745 (Wald $\chi^2 = 5.695$, $p = 0.017$; Fig. 7A). This is predominantly driven by a grade shift
746 in OL:body allometry (Wald $\chi^2 = 8.257$, $p = 0.004$; Fig. 8B) rather than in
747 midbrain:body allometry (Wald $\chi^2 = 3.805$, $p = 0.051$; Fig. 8C). Hence, *H. erato* have
748 larger OL volumes relative to body size than *H. hecale*. The same pattern is observed
749 in old insectary-reared individuals suggesting this is not an environmentally induced
750 difference (midbrain: Wald $\chi^2 = 1.721$, $p = 0.189$; OL Wald $\chi^2 = 11.131$, $p < 0.001$).
751 Among segmented neuropils only the La and Me show significant absolute
752 volumetric differences between wild-caught individuals of the two species, both being
753 larger in *H. hecale* (Table 4A). Analyses of allometric relationships imply species
754 differences in neuropil investment (Table 4A). La and Me show strong major-axis
755 shifts and we identify evidence for grade-shifts between rMid and aMe, Lob, LoP and
756 OG, as well as all segmented neuropil in the midbrain except the PB and POTu (Table
757 4A). In all of these cases the shift is towards larger relative volumes in *H. erato*, and
758 may be partially driven by the differences in rMid volume which is significantly
759 larger in *H. hecale* ($t_{17} = 3.582$, p = 0.002. $r = 0.656$). Only one neuropil, the AL,
760 shows evidence for a difference in the allometric coefficient β between species. The
761 AL scales with a significantly higher coefficient in *H. erato* ($\beta = 1.197$, 95% C.I. =
762 0.699–2.05) than *H. hecale* ($\beta = 0.470$, 95% C.I. = 0.313–0.705), indicating the ALs
763 of *H. erato* show a greater proportional increase in size as rMid increases than in *H.*
764 *hecale*.
765 Species differences between old insectary-reared individuals are notably less
766 widespread (Table 4B). The La is the only neuropil with a significant absolute
767 volumetric difference between species, and notably rMid volume is also not

768 significantly different (t_{17} = -1.391, p = 0.181). There is no evidence for species
769 differences in scaling coefficients for AL, and grade-shifts are restricted to Lam, Me,
770 and OG. However, the direction of the grade-shifts indicates *H. hecale* have relatively
771 larger component volumes. The difference in results between wild and old insectary-
772 reared individuals is most probably explained by species differences in environment-
773 dependent changes in rMid volume. The expanded rMid volume in wild individuals
774 masks the grade-shifts observed in La and Me in old insectary-reared individuals and,
775 because other segmented neuropil do not show a similar expansion, lead to the wide-
776 spread grade-shifts observed between wild caught *H. hecale* and *H. erato*. The effect
777 is even sufficient to reverse the direction of grade-shift for CB and LoP. These results
778 imply role for environmentally induced plasticity in contributing to species
779 differences, but also indicate environment-independent differences exist.
780 Discrimant Function Analysis (DFA) of component volumes is able to
781 distinguish wild individuals of the two species along one major axis, correctly
782 assigning 100% of samples to the correct species (Fig. 8D). Wilks Lambda suggests
783 group differences explain 90% of total variance between samples, although the formal
784 statistical test for a group difference does not reach significance (χ^2 = 20.76, 14
785 degrees of freedom, p = 0.108). To test whether phenotypic differentiation between
786 species is caused by both environmentally independent and dependent variation we
787 performed an additional DFA using four data-groups: i) wild *H. erato*, ii) old
788 insectary-reared *H. erato,* iii) wild *H. hecale*, iv) old insectary-reared *H. hecale*. This
789 analysis reduced the variation along three axes (Table 5A,B; Fig. 8E,F) which assign
790 87.2% of individuals to the correct data-group. No individuals were assigned to the
791 wrong species, incorrect assignment always occurred between wild and old groups of
792 the same species.
793 We subsequently performed a MANOVA to test for whether DF1, DF2 and
794 DF3 are associated with species and/or group (wild vs. old), and to test for significant
795 species-group interactions (Table 6C). DF1 showed a significant association with both
796 species and group, DF2 and DF3 were specifically associated with group. Only DF2
797 showed a significant species by group interaction. Visual inspection of Discrimant
798 Function plots (Fig. 8E,F) suggests DF2 separates wild and old insectary-reared
799 individuals more effectively in *H. hecale*.
800
801 **Divergence in brain composition across Lepidoptera and other insects**

Beyond *Heliconius* there is a clear signature of adaptive divergence in the composition of Lepidoptera brains. We combined the data collected for the present analysis with comparable volumetric data for eight neuropils from four other species (as collated in Montgomery and Ott, 2015, Table 3; Fig. 9A). After correcting for allometric scaling, using phylogenetically-corrected regressions against total neuropil volume, the six species can be separated along two principal components that together explain 90.7% of variance. PC1 is heavily loaded by sensory neuropil in the negative direction, and the MB-ca and MB-lo+ped in the positive direction (Table 6). PC2 is heavily loaded by the Me in the positive direction and the AL and CB in the negative direction. This separates the six species into three pairs, representing (i) *H. hecale* and *H. erato*; (ii) the other diurnal butterflies, *D. plexippus* and *G. zavaleta*); and (iii) the night-flying moths, *H. virescens* and *M. sexta* (Fig. 9B). When midbrain neuropil are analyzed separately, PC1, which explains 68.7% of variance, marks an axis dominated by the AL, CB and MB components. PC2, which explains an addition 23.3% variance, is strongly loaded by the AOTu (Fig. 9C). This leads to two clusters grouping (i) *H. hecale* and *H. erato*, which invest heavily in mushroom body neuropil, and (ii) the night-flying moths and *G. zavaleta*, which invest heavily in olfactory neuropil; leaving *D. plexippus* isolated by its large AOTu volume. Although this could be partially explained by the AOTu appearing small in *Heliconius* due to the expanded mushroom bodies, when the MB volume is removed from total midbrain, *D. plexippus* still has the largest residual AOTu size, suggesting this is a genuine signal of divergence. Whether the larger AOTu volume in *D. plexippus* is derived, or more typical for diurnal butterflies, is not known.

Finally, we consider the most notable adaptation in *Heliconius* brains, the increase in mushroom body volume, in a wider phylogenetic context. The combined volume of the calyx, pedunculus and lobes accounts for 13.7% of total brain neuropil volume in *H. erato*, and 11.9% in *H. hecale*. This is much larger than reported for any other Lepidoptera measured with similar methods (range 2.3-5.1%). Expressed as a percentage of the midbrain, to remove the effects of variation in the large OL, *H. erato* (38.5%) and *H. hecale* (32.9%) again exceed other Lepidoptera (4.8-13.5%) by 3–7 fold. These figures are also much larger than reported for *H. charithonia* (4.2% of total brain size) by Sivinski (1989), whose figures for other Lepidoptera are also much lower suggesting the difference is probably explained by variation in methodology. However, Sivinski reported the mushroom bodies of *H. charithonia* to

836 be approximately 4-times larger than those of the other butterflies measured, which is
837 similar to the fold differences we observe here.
838 Comparisons beyond Lepidoptera are complicated by differences in the
839 neuropil measured. For example, the total neuropil volume is not reported for the
840 *Tribolium* (Dreyer et al., 2010), *Leucophaea* (Wei et al., 2010) or *Drosophila* (Rein et
841 al., 2002) brains, which instead report individual neuropil volumes as a percentage of
842 the sum of all segmented components. The most well matched comparisons are to
843 *Apis mellifera* (Brandt et al., 2005) and *Schistocerca gregaria* (Kurylas et al., 2008)
844 for which mushroom body volume and midbrain volume are reported (Fig. 9D). Even
845 here, however, the data is not fully comparable, as the SOG is not fused with the
846 midbrain in *S. gregaria*. In *A. mellifera* the mushroom bodies comprise 65.4% of the
847 midbrain, (40.6% MB-ca, 24.8% MB-lo+ped) (Brandt et al., 2005), in gregarious-
848 phase *S. gregaria* they comprise 15.1% (8.2% MB-ca including the accessory calyx,
849 6.3% MB-lo+ped) (Kurylas et al., 2008). Ott and Rogers (2010) report proportional
850 calyx volumes in *S. gregaria* of 7.6% and 8.6% in solitarious-phase and gregarious-
851 phase locusts, respectively (both figures include the accessory calyx), but did not
852 measure the peduncle. In terms of raw volume our estimates (Table 1) *Heliconius*
853 mushroom bodies are roughly equal in size to *A. mellifera*.
854 More general comparisons can be made expressing mushroom body size as a
855 percentage of segmented neuropil (Me+Lobula system, CB, MB and AL) that were
856 labeled across a wider range species (Dreyer et al., 2010). In this analyses *A.*
857 *mellifera*, *T. castaneum* and *L. madera* all devote a larger proportion of total neuropil
858 to the mushroom bodies than *Heliconius*. However, they also have substantially
859 smaller optic lobes. If one instead examines the ratio of percentage mushroom body
860 volume to the percentage of the two other midbrain neuropil (AL and CB), *Heliconius*
861 have the largest ratios (*H. erato*: 6.4; *H. hecale*: 6.7) by some way, exceeding even *A.*
862 *mellifera* (3.8). Similarly, the residuals from the highly significant ($p < 0.001$) PGLS
863 regression (Fig. 9E) between percentage OL and percentage MB for *Heliconius* (*H.*
864 *erato* +8.2; *H. hecale* +7.5) are only exceeded by *A. mellifera* (+11.9), which both far
865 exceed the forth-largest residual (*S. gregaria* +2.2). A similar result is found
866 comparing percentage MB to percentage AL+CB. This fairly crude analysis at least
867 demonstrates that *Heliconius* rank highly across insects in terms of investment in
868 mushroom body neuropil.
869

DISCUSION

We have described the layout and volume of the major neuropils in the brain of two species of *Heliconius* butterflies. We have further demonstrated patterns of variation across age groups of insectary-reared and wild individuals that are consistent with significant post-eclosion growth and experience-dependent plasticity in neuropil volume. Our analyses confirm previous reports of a substantial expansion in mushroom body size during the evolution of *Heliconius* butterflies (Sivinski, 1989). Indeed, our data suggest this previous work underestimated the proportional size of the *Heliconius* mushroom bodies. We further demonstrate levels of plasticity in mushroom body volume comparable to those found in foraging insects known for their capacity to learn spatial information (e.g. Withers et al., 1993, 2008; Gronenberg et al., 1996; Fahrbach et al., 1998, 2003; Maleszka et al., 2009; Jones et al., 2013). However, plasticity is not limited to the mushroom bodies, nor is the signal of adaptive divergence in neuropil structure. In the following, we discuss how and why *Heliconius* may have evolved such large mushroom bodies, what the convergent expansion of the mushroom body in independent insect lineages can tell us about their function and significance, and finally widen our scope to consider how the brains of different Lepidoptera are adapted to their different ecological niches.

Mushroom body expansion in Heliconius

As a percentage of total brain volume, or indeed as a raw volume, *Heliconius* have the largest mushroom body so far reported in Lepidoptera (Sivinski, 1989; Sjöholm et al., 2005; Rø et al., 2007; Kvello et al., 2009; Snell-Rood et al., 2009; Dreyer et al., 2010; Heinze and Reppert, 2012b; Montgomery and Ott, 2015). The expansion affects the calyx, pedunculus and lobes. The calyx has an expanded double-lobe, deeply cupped structure, superficially reminiscent of the mushroom body calyx of *A. mellifera* (Brandt et al., 2005), but structurally quite different from the calyx of *Danaus plexippus* which is composed of a series of concentric sub-structures that are not deeply cupped. As in *D. plexippus* (Heinze and Reppert, 2012) and to a lesser extent *Godyris zavaleta* (Montgomery and Ott, 2015), the lobe system is sufficiently expanded to merge individual lobes that are distinct in *Manduca sexta* and *Heliothis virescens* (Sjöholm et al., 2005; Rø et al., 2007; El Jundi et al., 2009; Kvello et al.,

903 2009). This precludes an accurate assessment of whether all lobes are equally
904 expanded with the current data, which would be of interest given their relationship to
905 different aspects of memory (Krashes et al., 2007; Guven-ozkan and Davis, 2014;
906 Stopfer, 2014). It appears likely however that both the α'/β' and α/β lobes, which are
907 responsible for consolidating long-term memory, and for the retrieval and expression
908 of these memories (Guven-ozkan and Davis, 2014), contribute to the expansion.
909 Mushroom body expansion suggests the presence of selection for greater
910 memory capacity during *Heliconius* evolution. The unique pollen-feeding behavior of
911 adult *Heliconius*, and associated demands of foraging for spatially distributed
912 resources, provides the most likely source of this selection pressure (Gilbert, 1975;
913 Sivinski, 1989). Several studies have reported evidence of spatially and temporally
914 faithful foraging patterns (Ehrlich and Gilbert, 1973; Gilbert, 1975, 1993; Mallet,
915 1986) comparable with the well described trap-lining behavior of foraging bees
916 (Janzen, 1971; Heinrich, 1979). In hymenoptera, this behavior involves landmark
917 based spatial memory (Cartwright and Collett, 1983; Dyer, 1991; Menzel et al.,
918 2005). Mushroom bodies are implicated in spatial memory both through experimental
919 manipulation (Mizunami et al., 1998) and comparative neuro-ecological studies
920 (Farris and Schulmeister, 2011), although the role selection for spatial memory played
921 in mushroom body expansion in Hymenoptera remains unproven for some authors
922 (Menzel, 2014).
923 Comparisons across *Heliconius* and non-pollen feeding genera in the
924 Heliconiini may provide a test of this hypothesis. Sivinski (1989) reported that two
925 individuals of *Dione juno* and *Dryas iulia*, both non-pollen feeding allies to
926 *Heliconius*, have mushroom bodies within the range of other Lepidoptera. This
927 provides preliminary support that mushroom body expansion may have occurred co-
928 incidentally with a single origin of pollen feeding at the base of *Heliconius*. However,
929 several genera were not sampled, including the specious genus *Euides* which is most
930 closely related to *Heliconius* (Beltrán et al., 2007; Kozak et al., 2015). As such,
931 further sampling is required to confirm this conclusion. This work is underway. It is
932 also conceivable alternative selection pressures may play a role, such as the degree of
933 host-plant specialization (Brown, 1981) or the evolution of social roosting (Benson,
934 1972; Mallet, 1986). It is possible these factors are inter-related, as *Passiflora* may be
935 incorporated into trap-lines between pollen plants (Gilbert, 1975, 1993), and the
936 sedentary home-range behavior required for trap-lining may predispose *Heliconius* to

937 sociality (Mallet, 1986). Indeed, Farris and Schulmeister (2010) suggest sociality in
938 hymenoptera is an exaptation, dependent on the co-option of a pre-existing
939 elaboration of the mushroom bodies in response to the demands for spatial foraging in
940 parasitic Euhymenopteran. Similar hypotheses have been proposed in vertebrates, for
941 example, the initial expansion of the primate brain may have been driven by visual
942 specialization (Barton, 1998). Social intelligence may therefore be viewed as an
943 exaptation of this initial expansion that facilitated processing of a greater range and
944 complexity of information (Barton and Dunbar, 1997).

945 It is certainly likely that pollen feeding at least plays a role in meeting the
946 energetic costs of increased neural investment, even if it does not explain its origin.
947 Increased investment in both the neural tissue required for learning-based foraging
948 (Aiello et al., 1995; Laughlin et al., 1998; Snell-Rood et al., 2009) and the act of
949 learning itself (Mery and Kawecki, 2004; Burger et al., 2008; Snell-Rood et al., 2009,
950 2011) will impose significant energetic costs, potentially resulting in trade-offs
951 against other traits (Dukas, 1999; Burns et al., 2011; Snell-Rood et al., 2011; Snell-
952 Rood, 2013). The fitness benefits of pollen-feeding lie in increased longevity without
953 reproductive senescence (Dunlap-Pianka et al., 1977), facilitating a shift in the
954 energetic costs of chemical defense to larvae as adults are no longer dependent on
955 larval fat body stores (Cardoso and Gilbert, 2013), and amino acid transfer to eggs
956 (O'Brien et al., 2003). These combined effects must outweigh the energetic costs
957 incurred by greater neuropil investment.
958
959 ***Post-eclosion growth in mushroom body volume***
960 *Heliconius* are not as robust to environmental perturbation, or as amenable as
961 experimental subjects, as honeybees and ants. As a result our conditions are perhaps
962 less controlled than comparable studies in these insects. Nevertheless, there is a clear
963 effect of age on mushroom body size (Fig. 6). In both species, the mushroom bodies
964 are significantly larger in aged individuals. These volume differences of 38.0% for the
965 calyx and 34.0% for the lobe system in *H. erato,* and 27.9% for the calyx and 23.7%
966 for the lobe system in *H. hecale* are comparable, if not greater than, the effects seen in
967 Hymenoptera (e.g. c. 30% in *Camponotus floridanus* (Gronenberg et al., 1996); c.
968 20% in *Bombus impatiens* (Jones et al., 2013)).

969 Our comparisons between aged insectary-reared individuals and wild caught
970 individuals also identify experience-dependent plasticity. This 'experience' in the

971 wild likely includes a greater range of movement as well as a greater complexity of
972 foraging, and more variable environmental conditions and social interactions. In both
973 species we see evidence for mushroom body plasticity, however it is notable that the
974 pattern differs between species. In *H. hecale* a strong volumetric difference is found
975 between old insectary-reared and wild caught individuals for both the calyx (32%
976 difference) and lobes (24% difference). Again, this is a result of a major-axis shift in
977 the unsegmented midbrain. This is not just an effect of increases in total brain size, as
978 no other neuropil shows a similar increase resulting in widespread grade-shifts
979 towards smaller relative size in wild caught individuals. This may suggest a
980 coordinated pattern of growth between the mushroom bodies and unsegmented areas
981 of the midbrain or alternatively independent plasticity in the two structures. In *H.*
982 *erato* the effect of environmental plasticity is somewhat different. Although we find
983 similar volumes in old insectary-reared individuals and wild caught individuals, both
984 the mushroom body clayx and lobe system show allometric grade-shifts resulting in
985 greater volumes relative to the unsegmented midbrain in wild individuals compared to
986 insectary-reared individuals. It is also notable that this grade-shift is apparent because,
987 in contrast to *H. hecale*, *H. erato* does not show a concomitant increase in midbrain
988 volume in wild individuals.
989 It is currently unclear what causes this species difference. The difference may
990 reflect changes in connectivity between the mushroom bodies and neuropil housed in
991 the unsegmented midbrain, or perhaps experience-dependent plasticity in unrelated
992 midbrain structures. Alternatively, the difference may be a sampling artifact.
993 Although the ages of the insectary-reared individuals are not significantly different,
994 we cannot rule out that the age structure of wild-caught individuals is biased. A
995 further possibility is that *H. erato* and *H. hecale* respond differently to conditions in
996 captivity, perhaps due to contrasting natural behavior in the wild. Nevertheless, our
997 observation that *Heliconius* mushroom bodies show similar levels of post-eclosion
998 growth to Hymenoptera, and a similar two-phase pattern of environmentally
999 independent and dependent growth, provides further evidence of evolutionary
1000 convergence with *Heliconius*.
1001 These large, volumetric changes in mushroom body size presumably have
1002 some significance on how the mushroom bodies are functioning. Some insight into
1003 the functional significance may be gained from investigating what is causing the
1004 increase in volume. Ongoing proliferation of Kenyon cells seems unlikely, if

neurogenesis is restricted to the larval and pupal stages, as it is in Hymenoptera (Masson, 1970; Fahrbach et al., 1995). Instead the increased volume may indicate changes in dendritic growth, as is suggested for mushroom body plasticity in Hymenoptera (Gronenberg et al., 1996; Farris et al., 2001). Farris et al. (2001) demonstrated age and experience dependent plasticity in dendrite branching. The former reflecting developmentally programmed growth of extrinsic neuron processes into the mushroom bodies, and the latter reflecting an expansion in the complexity of Kenyon cell processes. The resulting changes in dendritic fields may indicate altered neural connectivity.

Finally, although the mushroom bodies show the strongest and most consistent effects, it is also striking that plasticity, and in particularly age related growth, is not restricted to the mushroom bodes. This has been observed in other insects (Kühn-Bühlmann and Wehner, 2006; Snell-Rood et al., 2009; Ott and Rogers, 2010; Smith et al., 2010; Heinze and Florman, 2013; Jones et al., 2013). As in previous examples significant age-dependent effects in *Heliconius* appear to play a role in the development of sensory neuropil involved in the processing of both visual and olfactory information. This may not be unexpected as sensory neuropil do not merely relay information on to the central brain, but also process information *in situ* (Muscedere et al., 2014). Both the medulla and lobula system are implicated in processing different types of visual information (Paulk et al., 2009a; b). Similarly, odor learning may be due to plasticity in the antennal lobes themselves rather than, or as well as, higher order structures (Hammer and Menzel, 1998; Rath et al., 2011). We also find evidence of plasticity in the central complex. In Lepidoptera, the plasticity in central body has been demonstrated in response to experience with novel host plants (Snell-Rood et al., 2009), whilst the protocerebral bridge increases in volume following migratory experience in *D. plexippus* (Heinze et al., 2013). Our results suggest *Heliconius* may provide a useful system within which to explore the behavioral relevance of plasticity in the mushroom bodies, and other structures.

Convergent expansion of mushroom bodies: similarities and differences

Extensive mushroom body expansion is now reported in lineages of four insect orders; Dictyoptera, herbivorous Scarabaeidae, Hymenoptera, and *Heliconius* (Farris, 2013). We see three ecological traits that are shared by at least two of these lineages: dietary adaptations, central place foraging, and sociality. In scarab beetles mushroom

body expansion is associated with a shift from coprophagy to a generalist phytophagus diet, possibly in response to increased behavioral flexibility in the context of foraging (Farris and Roberts, 2005). It is conceivable a similar selection pressure may apply to cockroaches. In contrast, the initial increase in mushroom body size coincides with the origin of a specialist foraging behavior in Hymenoptera, parasitoidism (Farris and Schulmeister, 2011). As discussed above, the expansion of the *Heliconius* mushroom bodies may also be related to a specialist foraging behavior. In these cases, central place foraging may have facilitated the origin of more social behavior (Mallet, 1986; Farris and Schulmeister, 2011), which may have secondarily led to further increases in mushroom body volume (Dujardin, 1859; Withers et al., 1993; Gronenberg et al., 1996; Ehmer and Ron, 1999). The common theme of these hypotheses is that mushroom body expansion evolves in response to the need for parsing a greater complexity of environmental information, facilitating the emergence of new behaviors (Chittka and Niven, 2009).

Two anatomical traits associated with mushroom body expansion provide support for this hypothesis: increased complexity of sensory input into the mushroom bodies, and subdivision of the mushroom body calyx. In addition to olfactory inputs, the mushroom body calyx receives direct input from the optic lobes in Hymenoptera and phytophagus Scarab beetles (Gronenberg, 2001; Farris and Roberts, 2005; Farris and Schulmeister, 2011). This increase in functional inputs is reflected in the subdivision of the calyx into the lip, which processes olfactory information, and the collar and basal ring, which process visual information (Gronenberg and Hölldobler, 1999). This suggests mushroom body expansion may be partly caused by the acquisition of new functions (Farris, 2013).

It is not known whether *Heliconius* receive visual input into the mushroom bodies. However, this has been demonstrated in species of both butterflies (Snell-Rood et al., 2009) and moths (Sjöholm et al., 2005), and some anatomical features of the *Heliconius* brain suggest the possibility that this does occur. It is notable, however, that *Heliconius* lack clear subdivision of the calyx as seen in Hymenoptera. In contrast, Heinze and Reppert (2012) described clear structural subdivision, or zonation, that they postulated may be analogous to the *A. mellifera* lip, collar and basal ring. We do not interpret the lack of clear zonation in *Heliconius* as evidence that there is no functional sub-division, as *Spodptera littoralis* displays localization of visual processing in the mushroom body calyx that is not apparent without labeling

individual neurons. Given the implied role for visual landmark learning in *Heliconius* foraging behavior (Jones, 1930; Gilbert, 1972, 1975; Mallet, 1986), it seems probable that there has been some integration of visual information processing with the mushroom bodies.

In other species the mushroom body also receives input relaying gustatory and mechanosensory information (Schildberger, 1983; Homberg, 1984; Li and Strausfeld, 1999; Farris, 2008). These may also be of relevance in *Heliconius* given the importance of gustatory and mechanosensory reception in host-plant identification (Schoonhoven, 1968; Renwick and Chew, 1994; Briscoe et al., 2013) and pollen loading (Krenn and Penz, 1998; Penz and Krenn, 2000), although it should be noted that there is currently no evidence these behaviors are learnt (Kerpel and Moreira, 2005; Salcedo, 2011; Silva et al., 2014).

Ecological adaptations in Lepidopteran brain composition

The mushroom body is not the only neuropil to display an adaptive signature of divergence. Our interspecific analysis across Lepidoptera strongly suggest a mosaic pattern of brain evolution (Barton and Harvey, 2000) in response to a species' specific ecological needs (Barton et al., 1995; Huber et al., 1997; Gronenberg and Hölldobler, 1999b; Montgomery and Ott, 2015). This pattern is particularly noticeable in the sensory neuropil (Fig. 9B). The relative volume of the visual neuropil closely reflects diel activity patters, whilst the size of the antennal lobe also appears to be strongly associated with activity pattern or a low-light diurnal niche. This is illustrated in a PCA of midbrain neuropil (Fig. 9C) which clusters the olfactorily driven butterfly *G. zavaletta* with night-flying moths (Montgomery and Ott, 2015). As expected, *Heliconius* are distinguished by their enlarged mushroom bodies, whilst *D. plexippus* is isolated along an axis of variation heavily loaded by the AOTu. This may reflect dependence on visual information typical of diurnal butterflies; however, removal of the mushroom bodies from the analysis does not explain this difference. It is possible therefore that AOTu expansion is particularly prominent in *D. plexippus* as suggested by Heinze and Reppert (2012). The AOTu plays a key role in relaying segregated visual pathways (Pfeiffer et al., 2005; Heinze and Reppert, 2011; Mota et al., 2011; Pfeiffer and Kinoshita, 2012), suggesting a plausible link between AOTu expansion and migratory behavior (Heinze and Reppert, 2012a; Heinze et al., 2013).

These macroevolutionary patterns of divergence between genera are mirrored to some extent in comparisons between *H. erato* and *H. hecale*. In Panama, *H. hecale* and *H. erato* differ in host-plant use (Merrill et al., 2013), and *H. hecale* are biased towards collecting large grained pollen whereas *H. erato* collect pollen from plant species that produce smaller grains (Estrada and Jiggins, 2002). Although this may reflect foraging differences, it is likely that the difference is largely driven by competitive exclusion of *H. erato* from a generally preferred pollen source (Estrada and Jiggins, 2002) as there is no difference in the efficiency of handling different pollen sizes in captivity (Penz and Krenn, 2000), or evidence that *H. erato* preferentially collect small pollen grains in other wild populations (Boggs et al., 1981; Cardoso, 2001). These data suggest *H. erato* and *H. hecale* may be using their environment differently, and therefore be exposed to contrasting conditions and selection pressures.

Focusing on wild caught individuals, where variation in neuropil volume may be most ecologically relevant, *H. hecale* have a significantly larger total brain size. This is largely due to the optic lobes, and undefined regions of the midbrain. At the level of specific neuropil only the lamina and medulla differ significantly between species. However, interpreting allometric grade-shifts between species is complicated by significant differences in unsegmented midbrain volume, which is used as the independent variable throughout. In old insectary-reared individuals the significant difference in lamina volume persists, suggesting this may be a non-plastic species difference, whilst the effects on midbrain volume may be environment dependent. This supports recent data showing divergence in corneal facet number and diameter which suggests visual adaptations in different micro-habitats may play a role in *Heliconius* diversification (Seymoure et al., in review).

The behavioral relevance of divergence and plasticity in unsegmented areas of the midbrain, which lack clear boundaries, is less obvious. Given its role in controlling the mandibles, proboscis and mouth parts (Rehder, 1989; Bowdan and Wyse, 2000), all of which are involved in pollen loading (Krenn and Penz, 1998; Penz and Krenn, 2000), it is possible the effect is largely driven by variation in the sub-esophageal ganglion caused by species differences in pollen handling in the wild. The development of phenotypic markers that permit consistent segmentation of different areas of the midbrain across species (e.g. Heinze and Reppert, 2012) in future studies will permit a test of this hypothesis.

Interspecific differences between *H. erato* and *H. hecale* in brain component volumes are sufficient to correctly group individuals by species in a discriminant function analysis. Further analysis of species and group (wild vs. old insectary-reared) suggest both environment independent and dependent variation contributes to these species differences. The potential role of phenotypic plasticity in facilitating ecological diversification by bridging fitness valleys is attracting renewed and growing interest (Pfennig et al., 2010; Snell-Rood, 2013). The numerous closely related sister-species of *Heliconius* that exist along environmental gradients (Jiggins et al., 1996; Jiggins and Mallet, 2000; Estrada and Jiggins, 2002; Arias et al., 2008) may provide an opportunity to test the importance of neural phenotypic plasticity in facilitating ecological shifts during speciation.

Conclusions and future prospects

We have described the layout and size of the major neuropil in two species of *Heliconius* butterflies. This has confirmed a previous report that this genus has dramatically expanded mushroom bodies (Sivinski, 1989). Moreover our estimates of the percentage of the brain occupied by the mushroom bodies suggest the initial values underestimated the size of the mushroom body. Indeed, in some comparisons, *Heliconius* rank among the top insect species in terms of investment in mushroom body neuropil. Through comparisons across different age groups, and between wild and insectary-reared individuals, we further demonstrate levels of plasticity comparable to hymenoptera, extensively studied models of mushroom body expansion and plasticity. Our interspecific analysis reveals patterns of divergence in brain composition between genera, and within *Heliconius*, that suggest a close correspondence to ecological variables. This analysis lays the groundwork for comparative and experimental analyses that will seek to dissect the costs, benefits, behavioral relevance and proximate basis of differential expansion in key neuropil.

Other acknowledgments

The authors are grateful to Adriana Tapia, Moises Abanto, William Wcislo, Owen McMillan, Chris Jiggins, and the Smithsonian Tropical Research Institute for assistance, advice, and the use of the *Heliconius* insectaries at Gamboa, Panama, and the Ministerio del Ambiente for permission to collect butterflies in Panama. We also

thank Judith Mank's research group at UCL for helpful advice and feedback, and the UCL Imaging Facility for help with confocal microscopy.

Conflict of interest statement

The authors declare no conflict of interest.

Role of authors

All authors read and approved the final manuscript. Study conception: SHM. Study design and preliminary experiments: SHM, RMM, SRO. Fieldwork and insectary rearing: SHM, RMM. Acquisition of data, analysis, interpretation and initial manuscript draft: SHM. Final interpretation and drafting: SHM, RMM, SRO.

Literature cited

Aiello LC, Wheeler P. 1995. The expensive-tissue hypothesis: the brain and the digestive system in human and primate evolution. Curr Anthropol 199–221.

Arias CF, Muñoz AG, Jiggins CD, Mavárez J, Bermingham E, Linares M. 2008. A hybrid zone provides evidence for incipient ecological speciation in Heliconius butterflies. Mol Ecol 17:4699–712.

Barton RA, Harvey PH. 2000. Mosaic evolution of brain structure in mammals. Nature 405:1055–1058.

Barton RA. 1998. Visual specialization and brain evolution in primates. Proc Biol Sci 265:1933–1937.

Barton RA, Dunbar RI. 1997. Evolution of the social brain. In: Whiten A, Byrne RW, editors. Machiavellian intelligence II: Extensions and evaluations. Cambridge University Press. p 240.

Barton RA, Purvis A, Harvey PH. 1995. Evolutionary radiation of visual and olfactory brain systems in primates, bats and insectivores. Philos Trans R Soc Lond B Biol Sci 348:381–92.

Beltrán M, Jiggins CD, Brower AVZ, Bermingham E, Mallet J. 2007. Do pollen feeding , pupal-mating and larval gregariousness have a single origin in *Heliconius* butterflies? Inferences from multilocus DNA sequence data. J Linn Soc 92:221–239.

Benson WW. 1972. Natural selection for Miillerian mimicry in *Heliconius erato* in Costa Rica. Science (80) 176:936–939.

1207 Berg BG, Galizia CG, Brandt R, Mustaparta H. 2002. Digital atlases of the antennal
1208 lobe in two species of tobacco budworm moths, the Oriental *Helicoverpa assulta*
1209 (male) and the American *Heliothis virescens* (male and female). J Comp Neurol
1210 446:123–134. A

1211 Boeckh J, Boeckh V. 1979. Threshold and odor specificity of pheromone-sensitive
1212 neurons in the deutocerebrum of *Antheraea pernyi* and *A. polyphemus*
1213 (Saturnidae). J Comp Physiol A 132:235–242.

1214 Boggs CL, Smiley JT, Gilbert LE. 1981. Patterns of pollen exploitation by *Heliconius*
1215 butterflies. Oecologia 48:284–289.

1216 Bowdan E, Wyse GA. 2000. Temporally patterned activity recorded from mandibular
1217 nerves of the isolated subesophageal ganglion of *Manduca*. J Insect Physiol
1218 46:709–719.

1219 Brandt R, Rohlfing T, Rybak J, Krofczik S, Maye A, Westerhoff M, Hege H-C,
1220 Menzel R. 2005. Three-dimensional average-shape atlas of the honeybee brain
1221 and its applications. J Comp Neurol 492:1–19.

1222 Briscoe AD, Macias-Muñoz A, Kozak KM, Walters JR, Yuan F, Jamie GA, Martin
1223 SH, Dasmahapatra KK, Ferguson LC, Mallet J, Jacquin-Joly E, Jiggins CD.
1224 2013. Female behaviour drives expression and evolution of gustatory receptors
1225 in butterflies. PLoS Genet 9:e1003620.

1226 Brown KS. 1981. The biology of *Heliconius*. Annu Rev Entomol 26:427–457.

1227 Burger JMS, Kolss M, Pont J, Kawecki TJ. 2008. Learning ability and longevity: A
1228 symmetrical evolutionary trade-off in *Drosophila*. Evolution 62:1294–1304.

1229 Burish MJ, Kueh HY, Wang SSH. 2004. Brain architecture and social complexity in
1230 modern and ancient birds. Brain Behav Evol 63:107–124.

1231 Burns JG, Foucaud J, Mery F. 2011. Costs of memory: lessons from “mini” brains.
1232 Proc Biol Sci 278:923–929.

1233 Capaldi EA, Robinson GE, Fahrback SE. 1999. Neuroethology of spatial learning: the
1234 birds and the bees. Annu Rev Psychol 50:651–682.

1235 Cardoso MZ, Gilbert LE. 2013. Pollen feeding, resource allocation and the evolution
1236 of chemical defence in passion vine butterflies. J Evol Biol 26:1254–60.

1237 Cardoso MZ. 2001. Patterns of pollen collection and flower visitation by *Heliconius*
1238 butterflies in southeastern Mexico. J Trop Ecol 17:763–768.

1239 Carlsson MA, Schäpers A, Nässel DR, Janz N. 2013. Organization of the olfactory
1240 system of Nymphalidae butterflies. Chem Senses 38:355–67.

1241 Cartwright BA, Collett TS. 1983. Landmark learning in bees - Experiments and
1242 models. J Comp Physiol A 151:521–543.

1243 Chittka L, Niven J. 2009. Are Bigger Brains Better? Curr Biol19:R995–R1008.

1244 Clayton NS, Krebs JR. 1995. Memory in food-storing birds: From behaviour to brain.
1245 Curr Opin Neurobiol 5:149–154.

1246 Cohen J. 1988. Statistical power analysis for the behavioral sciences. 2nd ed.
1247 Hillsdale, NJ.: Lawrence Earlbaum Associates.

1248 Dasmahapatra KK, Walters JR, Briscoe AD, Davey JW, Whibley A, Nadeau NJ,
1249 Zimin A V., Hughes DST, Ferguson LC, Martin SH, Salazar C, Lewis JJ, Adler
1250 S, Ahn S-J, Baker DA, Baxter SW, Chamberlain NL, Chauhan R, Counterman
1251 BA, Dalmay T, Gilbert LE, Gordon K, Heckel DG, Hines HM, Hoff KJ, Holland
1252 PWH, Jacquin-Joly E, Jiggins FM, Jones RT, Kapan DD, Kersey P, Lamas G,
1253 Lawson D, Mapleson D, Maroja LS, Martin A, Moxon S, Palmer WJ, Papa R,
1254 Papanicolaou A, Pauchet Y, Ray DA, Rosser N, Salzberg SL, Supple MA,
1255 Surridge A, Tenger-Trolander A, Vogel H, Wilkinson PA, Wilson D, Yorke JA,
1256 Yuan F, Balmuth AL, Eland C, Gharbi K, Thomson M, Gibbs RA, Han Y,
1257 Jayaseelan JC, Kovar C, Mathew T, Muzny DM, Ongeri F, Pu L-L, Qu J,
1258 Thornton RL, Worley KC, Wu Y-Q, Linares M, Blaxter ML, Ffrench-Constant
1259 RH, Joron M, Kronforst MR, Mullen SP, Reed RD, Scherer SE, Richards S,
1260 Mallet J, Owen McMillan W, Jiggins CD. 2012. Butterfly genome reveals
1261 promiscuous exchange of mimicry adaptations among species. Nature 487:94–8.

1262 Dreyer D, Vitt H, Dippel S, Goetz B, El Jundi B, Kollmann M, Huetteroth W,
1263 Schachtner J. 2010. 3D standard brain of the Red Flour Beetle *Tribolium*
1264 *castaneum*: A tool to study metamorphic development and adult plasticity. Front
1265 Syst Neurosci 4:3.

1266 Dujardin F. 1859. Mémoire sur le système nerveux des insectes. Ann Des Sci Nat
1267 comprenant la Zool 14:195–206.

1268 Dukas R. 1999. Costs of memory: ideas and predictions. J Theor Biol 197:41–50.

1269 Dunlap-Pianka H, Boggs CL, Gilbert LE. 1977. Ovarian dynamics in heliconiine
1270 butterflies: programmed senescence versus eternal youth. Science (80) 197:487–
1271 490.

1272 Durst C, Eichmüller S, Menzel R. 1994. Development and experience lead to
1273 increased volume of subcompartments of the honeybee mushroom body. Behav
1274 Neural Biol 62:259–263.

1275 Dyer F. 1991. Bees acquire route-based memories but not cognitive maps in a familiar
1276 landscape. Anim Behav 41:239–246.

1277 Edgar RC. 2004. MUSCLE: multiple sequence alignment with high accuracy and
1278 high throughput. Nucleic Acids Res 32:1792–7.

1279 Ehmer B, Ron H. 1999. Mushroom bodies of vespid wasps. J Comp Neurol 416:93–
1280 100.

1281 Ehrlich PR, Gilbert LE. 1973. Population structure and dynamics of the Tropical
1282 butterfly *Heliconius ethilla*. Biotropica 5:69–82.

1283 Estrada C, Jiggins CD. 2002. Patterns of pollen feeding and habitat preference among
1284 Heliconius species. Ecol Entomol 27:448–456.

1285 Fahrbach SE, Farris SM, Sullivan JP, Robinson GE. 2003. Limits on volume changes
1286 in the mushroom bodies of the honey bee brain. J Neurobiol 57:141–151.

1287 Fahrbach SE, Giray T, Robinson GE. 1995. Volume changes in the mushroom bodies
1288 of adult honey bee queens. Neurobiol Learn Mem 63:181–191.

1289 Fahrbach SE, Moore D, Capaldi EA, Farris SM, Robinson GE. 1998. Experience-
1290 expectant plasticity in the mushroom bodies of the honeybee. Learn Mem 5:115–
1291 123.

1292 Farris SM, Roberts NS. 2005. Coevolution of generalist feeding ecologies and
1293 gyrencephalic mushroom bodies in insects. Proc Natl Acad Sci U S A
1294 102:17394–17399.

1295 Farris SM, Robinson GE, Fahrbach SE. 2001. Experience- and age-related outgrowth
1296 of intrinsic neurons in the mushroom bodies of the adult worker honeybee. J
1297 Neurosci 21:6395–6404.

1298 Farris SM, Schulmeister S. 2011. Parasitoidism, not sociality, is associated with the
1299 evolution of elaborate mushroom bodies in the brains of hymenopteran insects.
1300 Proc Biol Sci 278:940–951.

1301 Farris SM. 2005. Evolution of insect mushroom bodies: old clues, new insights.
1302 Arthropod Struct Dev 34:211–234.

1303 Farris SM. 2008. Tritocerebral tract input to the insect mushroom bodies. Arthropod
1304 Struct Dev 37:492–503.

1305 Farris SM. 2013. Evolution of complex higher brain centers and behaviors: behavioral
1306 correlates of mushroom body elaboration in insects. Brain Behav Evol 82:9–18.

1307 Finkbeiner SD. 2014. Communal roosting in heliconius butterflies (Nymphalidae):
1308 roost recruitment, establishment, fidelity, and resource use trends based on age
1309 and sex. J Lepid Soc 68:10–16.

1310 Finlay B, Darlington R. 1995. Linked regularities in the development and evolution of
1311 mammalian brains. Science (80) 268:1578–1584.

1312 Garamszegi LZ, Eens M. 2004. The evolution of hippocampus volume and brain size
1313 in relation to food hoarding in birds. Ecol Lett 7:1216–1224.

1314 Gilbert LE. 1972. Pollen feeding and reproductive biology of *Heliconius* butterflies.
1315 Proc Natl Acad Sci USA 69:1403–1407.

1316 Gilbert LE. 1975. Ecological consequences of a coevolved mutualism between
1317 butterflies and plants. In: Gilbert LE, Raven P, editors. Coevolution of animals
1318 and plants. p 210–240.

1319 Gilbert LE. 1993. An evolutionary food web and its relationship to Neotropical
1320 biodiversity. In: W Barthlott, CM Naumann, K Schmidt-Loske, KL
1321 Schuchmann, editors. Animal-plant interactions in Tropical environments.
1322 Zoologisches Forschungsinstitut und Museum Alexander Koenig, Bonn,
1323 Germany. p 17–28.

1324 Giurfa M, Menzel R. 2001. Cognitive architecture of a mini-brain. Adapt Learn An
1325 Interdiscip Debate 5:22 – 48.

1326 Gonda A, Herczeg G, Merilä J. 2009a. Adaptive brain size divergence in nine-spined
1327 sticklebacks (*Pungitius pungitius*)? J Evol Biol 22:1721–1726.

1328 Gonda A, Herczeg G, Merilä J. 2009b. Habitat-dependent and -independent plastic
1329 responses to social environment in the nine-spined stickleback (*Pungitius*
1330 *pungitius*) brain. Proc Biol Sci 276:2085–2092.

1331 Gonda A, Herczeg G, Merilä J. 2013. Evolutionary ecology of intraspecific brain size
1332 variation: A review. Ecol Evol 3:2751–2764.

1333 Greenacre MJ. 2010. Biplots in practice. Fundacion BBVA.

1334 Gronenberg W, Heeren S, Hölldobler B. 1996. Age-dependent and task-related
1335 morphological changes in the brain and the mushroom bodies of the ant
1336 *Camponotus floridanus*. J Exp Biol 199:2011–9.

1337 Gronenberg W, Hölldobler B. 1999. Morphologic representation of visual and
1338 antennal information in the ant brain. J Comp Neurol 412:229–40.

1339 Gronenberg W. 2001. Subdivisions of hymenopteran mushroom body calyces by their
1340 afferent supply. J Comp Neurol 435:474–489.

1341 Guven-ozkan T, Davis RL. 2014. Functional neuroanatomy of *Drosophila* olfactory
1342 memory formation. :519–526.

1343 Hammer M, Menzel R. 1998. Multiple sites of associative odor learning as revealed
1344 by local brain microinjections of octopamine in honeybees. Learn Mem 5:146–
1345 156.

1346 Heinrich B. 1979. Resource heterogeneity and patterns of movement in foraging
1347 bumblebees. Oecologia 40:235–245.

1348 Heinze S, Florman J, Asokaraj S, El Jundi B, Reppert SM. 2013. Anatomical basis of
1349 sun compass navigation II: the neuronal composition of the central complex of
1350 the monarch butterfly. J Comp Neurol 521:267–98.

1351 Heinze S, Reppert SM. 2011. Sun compass integration of skylight cues in migratory
1352 monarch butterflies. Neuron 69:345–358.

1353 Heinze S, Reppert SM. 2012. Anatomical basis of sun compass navigation I: the
1354 general layout of the monarch butterfly brain. J Comp Neurol 520:1599–628.

1355 Hofbauer A, Ebel T, Waltenspiel B, Oswald P, Chen Y, Halder P, Biskup S,
1356 Lewandrowski U, Winkler C, Sickmann A, Buchner S, Buchner E. 2009. The
1357 Wuerzburg hybridoma library against *Drosophila* brain. J Neurogenet 23:78–91.

1358 Homberg U. 1984. Processing of antennal information in extrinsic mushroom body
1359 neurons of the bee brain. J Comp Physiol A Neuroethol Sens Neural Behav
1360 Physiol:825–836.

1361 Huber R, van Staaden MJ, S K Les, Liem KF. 1997. Microhabitat use, trophic
1362 patterns, and the evolution of brain structure in African Cichlids. Brain Behav
1363 Evol 50:167–182.

1364 Huetteroth W, Schachtner J. 2005. Standard three-dimensional glomeruli of the
1365 *Manduca sexta* antennal lobe: a tool to study both developmental and adult
1366 neuronal plasticity. Cell Tissue Res 319:513–24.

1367 Janzen ADH. 1971. Euglossine bees as long-distance pollinators of tropical plants.
1368 Science (80) 171:203–205.

1369 Jiggins C, Mallet J. 2000. Bimodal hybrid zones and speciation. Trends Ecol Evol
1370 15:250–255.

1371 Jiggins CD, Macmillan WO, Neukirchen W a. LT, Mallet J. 1996. What can hybrid
1372 zones tell us about speciation? The case of *Heliconius erato* and *H. himera*
1373 (Lepidoptera: Nymphalidae). Biol J Linn Soc 59:221–242.

1374 Jiggins CD. 2008. Ecological speciation in mimetic butterflies. Bioscience 58:541.

1375 Jones BM, Leonard AS, Papaj DR, Gronenberg W. 2013. Plasticity of the worker
1376 bumblebee brain in relation to age and rearing environment. Brain Behav Evol
1377 82:250–261.

1378 Jones F. 1930. The sleeping heliconias of Florida. Nat Hist 30:635–644.

1379 El Jundi B, Huetteroth W, Kurylas AE, Schachtner J. 2009. Anisometric brain
1380 dimorphism revisited: Implementation of a volumetric 3D standard brain in
1381 *Manduca sexta*. J Comp Neurol 517:210–25.

1382 Kazawa T, Namiki S, Fukushima R, Terada M, Soo K, Kanzaki R. 2009. Constancy
1383 and variability of glomerular organization in the antennal lobe of the silkmoth.
1384 Cell Tissue Res 336:119–36.

1385 Kerpel SM, Moreira GRP. 2005. Absence of learning and local specialization on host
1386 plant selection by *Heliconius erato*. J Insect Behav 18:433–452.

1387 Klagges BR, Heimbeck G, Godenschwege T a, Hofbauer a, Pflugfelder GO,
1388 Reifegerste R, Reisch D, Schaupp M, Buchner S, Buchner E. 1996. Invertebrate
1389 synapsins: a single gene codes for several isoforms in *Drosophila*. J Neurosci
1390 16:3154–65.

1391 Kozak KM, Wahlberg N, Dasmahapatra KK, Mallet J, Jiggins CD. 2015. Multilocus
1392 species trees show the recent adaptive radiation of the mimetic *Heliconius*
1393 butterlies. Syst Biol. *in press.*

1394 Krashes MJ, Keene AC, Leung B, Armstrong JD, Waddell S. 2007. Sequential use of
1395 mushroom body neuron subsets during *Drosophila* odor memory processing.
1396 Neuron 53:103–115.

1397 Krenn HW, Penz CM. 1998. Mouthparts of *Heliconius* butterflies (Lepidoptera :
1398 Nymphalidae): A search for anatomical adaptations to pollen-feeding behavior.
1399 Int J Insect Morphol Embryol 27:301–309.

1400 Kühn-Bühlmann S, Wehner R. 2006. Age-dependent and task-related volume changes
1401 in the mushroom bodies of visually guided desert ants, *Cataglyphis bicolor*. J
1402 Neurobiol 66:511–521.

1403 Kurylas AE, Rohlfing T, Krofczik S, Jenett A, Homberg U. 2008. Standardized atlas
1404 of the brain of the desert locust, *Schistocerca gregaria*. Cell Tissue Res
1405 333:125–45.

1406 Kvello P, Løfaldli BB, Rybak J, Menzel R, Mustaparta H. 2009. Digital, three-
1407 dimensional average shaped atlas of the *Heliothis virescens* brain with integrated
1408 gustatory and olfactory neurons. Front Syst Neurosci 3:14.

1409 Laughlin SB, de Ruyter van Steveninck RR, Anderson JC. 1998. The metabolic cost
1410 of neural information. Nat Neurosci 1:36–41.

1411 Li Y, Strausfeld NJ. 1997. Morphology and sensory modality of mushroom body
1412 extrinsic neurons in the brain of the cockroach, *Periplaneta americana*. J Comp
1413 Neurol 387:631–650.

1414 Li Y, Strausfeld NJ. 1999. Multimodal efferent and recurrent neurons in the medial
1415 lobes of cockroach mushroom bodies. J Comp Neurol 409:647–63.

1416 Lihoreau M, Latty T, Chittka L. 2012. An exploration of the social brain hypothesis in
1417 insects. Front Physiol 3:1–7.

1418 Maleszka J, Barron AB, Helliwell PG, Maleszka R. 2009. Effect of age, behaviour
1419 and social environment on honey bee brain plasticity. J Comp Physiol A
1420 Neuroethol Sensory, Neural, Behav Physiol 195:733–740.

1421 Mallet J. 1980. A laboratory study of gregarious roosting in the butterfly *Heliconius*
1422 *melpomene*. MSc Thesis. UCL Eprints no. 1301849
1423 (http://discovery.ucl.ac.uk/1301849)

1424 Mallet J. 1986. Gregarious roosting and home range in *Heliconius* butterflies. Natl
1425 Geogr Res. 2:198-215

1426 Mallet J. 1993. Speciation, raciation, and color pattern evolution in *Heliconius*
1427 butterflies: evidence from hybrid zones. In: Harrison RG, editor. Hybrid zones
1428 and the evolutionary process. Oxford University Press. p 226–260.

1429 Masante-Roca I, Gadenne C, Anton S. 2005. Three-dimensional antennal lobe atlas of
1430 male and female moths, *Lobesia botrana* (Lepidoptera: Tortricidae) and
1431 glomerular representation of plant volatiles in females. J Exp Biol 208:1147–59.

1432 Masson C. 1970. Mise en évidence, au cours de l'ontogénèse d'une fourmi primities
1433 (*Mesoponera caffraria* F.Smith), d'une prolifération tardive au niveau des
1434 cellules golbuleuses (Globuli-cells) des corps pedonculés. Z. Zllforsch 106: 220-
1435 231.

1436 Menzel R, Greggers U, Smith A, Berger S, Brandt R, Brunke S, Bundrock G, Hülse
1437 S, Plümpe T, Schaupp F, Schüttler E, Stach S, Stindt J, Stollhoff N, Watzl S.
1438 2005. Honey bees navigate according to a map-like spatial memory. Proc Natl
1439 Acad Sci USA 102:3040–3045.

1440 Menzel R. 2014. The insect mushroom body, an experience-dependent recoding
1441 device. J Physiol Paris 108:84–95.

1442 Merrill R et al. The diversification of *Heliconius* butterflies: what have we learned in
1443 150 years? J Evol Biol. *in review*

1444 Merrill R Naisbit RE, Mallet J, Jiggins CD. 2013. Ecological and genetic factors
1445 influencing the transition between host-use strategies in sympatric *Heliconius*
1446 butterflies. *J Evol Biol.* 26: 1959-1967.

1447 Mery F, Kawecki TJ. 2004. An operating cost of learning in *Drosophila*
1448 *melanogaster*. Anim Behav 68:589–598.

1449 Mizunami M, Weibrecht JM, Strausfeld NJ. 1998. Mushroom bodies of the
1450 cockroach: Their participation in place memory. J Comp Neurol 402:520–537.

1451 Molina Y, O'Donnell S. 2007. Mushroom body volume is related to social aggression
1452 and ovary development in the paperwasp *Polistes instabilis*. Brain Behav Evol
1453 70:137–144.

1454 Montgomery SH, Ott SR. 2015. Brain composition in *Godyris zavaleta* , a diurnal
1455 butterfly, reflects an increased reliance on olfactory information. J Comp Neurol
1456 523:869–891.

1457 Mota T, Yamagata N, Giurfa M, Gronenberg W, Sandoz J-C. 2011. Neural
1458 organization and visual processing in the anterior optic tubercle of the honeybee
1459 brain. J Neurosci 31:11443–11456.

1460 Müller F. 1879. Ituna and Thyridia: a remarkable case of mimicry in butterflies. Trans
1461 Entomol Soc Lond:20–29.

1462 Murawski DA, Gilbert LE. 1986. Pollen flow in *Psiguria warscewiczii*: a comparison
1463 of *Heliconius* butterflies and hummingbirds. Oecologia 68:161–167.

1464 Muscedere ML, Gronenberg W, Moreau CS, Traniello JF a. 2014. Investment in
1465 higher order central processing regions is not constrained by brain size in social
1466 insects. Proc Biol Sci 281:20140217.

1467 Neuser K, Triphan T, Mronz M, Poeck B, Strauss R. 2008. Analysis of a spatial
1468 orientation memory in *Drosophila*. Nature 453:1244–1247.

1469 Van Nouhuys S, Kaartinen R. 2008. A parasitoid wasp uses landmarks while
1470 monitoring potential resources. Proc Biol Sci 275:377–385.

1471 O'Brien DM, Boggs CL, Fogel ML. 2003. Pollen feeding in the butterfly *Heliconius*
1472 charitonia: isotopic evidence for essential amino acid transfer from pollen to
1473 eggs. Proc Biol Sci 270:2631–2636.

1474 O'Donnell S, Clifford MR, DeLeon S, Papa C, Zahedi N, Bulova SJ. 2013. Brain size
1475 and visual environment predict species differences in paper wasp sensory
1476 processing brain regions (hymenoptera: vespidae, polistinae). Brain Behav Evol
1477 82:177–84.

1478 Ofstad TA, Zuker CS, Reiser MB. 2011. Visual place learning in *Drosophila*
1479 *melanogaster*. Nature 474:204–207.

1480 Ott SR, Rogers SM. 2010. Gregarious desert locusts have substantially larger brains
1481 with altered proportions compared with the solitarious phase. Proc Biol Sci
1482 277:3087–96.

1483 Ott SR. 2008. Confocal microscopy in large insect brains: zinc-formaldehyde fixation
1484 improves synapsin immunostaining and preservation of morphology in whole-
1485 mounts. J Neurosci Methods 172:220–30.

1486 Pagel M. 1999. Inferring the historical patterns of biological evolution. Nature
1487 401:877–84.

1488 Park PJ, Bell MA. 2010. Variation of telencephalon morphology of the threespine
1489 stickleback (*Gasterosteus aculeatus*) in relation to inferred ecology. J Evol Biol
1490 23:1261–1277.

1491 Paulk AC, Dacks AM, Gronenberg W. 2009a. Color processing in the medulla of the
1492 bumblebee (Apidae: *Bombus impatiens*). J Comp Neurol 513:441–456.

1493 Paulk AC, Dacks AM, Phillips-Portillo J, Fellous J-M, Gronenberg W. 2009b. Visual
1494 processing in the central bee brain. J Neurosci 29:9987–9999.

1495 Penz CM, Krenn HW. 2000. Behavioral adaptations to pollen-feeding in *Heliconius*
1496 butterflies (Nymphalidaae, Heliconiinae): An experiment using *Lantana* flowers.
1497 J Insect Behav 13 :865–880.

1498 Pfeiffer K, Homberg U. 2014. Organization and functional roles of the central
1499 complex in the insect brain. Annu Rev Entomol 59:165–84.

1500 Pfeiffer K, Kinoshita M, Homberg U. 2005. Polarization-sensitive and light-sensitive
1501 neurons in two parallel pathways passing through the anterior optic tubercle in
1502 the locust brain. J Neurophysiol 94:3903–3915.

1503 Pfeiffer K, Kinoshita M. 2012. Segregation of visual inputs from different regions of
1504 the compound eye in two parallel pathways through the anterior optic tubercle of
1505 the bumblebee (*Bombus ignitus*). J Comp Neurol 520:212–229.

1506 Pfennig DW, Wund MA, Snell-Rood EC, Cruickshank T, Schlichting CD, Moczek
1507 AP. 2010. Phenotypic plasticity's impacts on diversification and speciation.
1508 Trends Ecol Evol 25:459–467.

1509 Plath OE. 1934. Bumblebees and their Ways. London, UK. The Macmillan Company.

1510 Pollen AA, Dobberfuhl AP, Scace J, Igulu MM, Renn SCP, Shumway CA, Hofmann
1511 H a. 2007. Environmental complexity and social organization sculpt the brain in
1512 Lake Tanganyikan cichlid fish. Brain Behav Evol 70:21–39.

1513 Rath L, Giovanni Galizia C, Szyszka P. 2011. Multiple memory traces after
1514 associative learning in the honey bee antennal lobe. Eur J Neurosci 34:352–360.

1515 Rehder V. 1989. Sensory pathways and motoneurons of the proboscis reflex in the
1516 suboesophageal ganglion of the honey bee. J Comp Neurol 279:499–513.

1517 Rein K, Zöckler M, Mader MT, Grübel C, Heisenberg M. 2002. The *Drosophila*
1518 standard brain. Curr Biol 12:227–31.

1519 Renwick JAA, Chew FS. 1994. Oviposition behavior in Lepidoptera. Annu Rev
1520 Entomol 39:377–400.

1521 Rø H, Müller D, Mustaparta H. 2007. Anatomical organization of antennal lobe
1522 projection neurons in the moth *Heliothis virescens*. J Comp Neurol 500:658–75.

1523 Rosenheim J a. 1987. Host location and exploitation by the cleptoparasitic wasp
1524 *Argochrysis armilla*: the role of learning (Hymenoptera: Chrysididae). Behav
1525 Ecol Sociobiol 21:401–406.

1526 Rospars JP. 1983. Invariance and sex-specific variations of the glomerular
1527 organization in the antennal lobes of a moth, *Mamestra brassicae*, and a
1528 butterfly, *Pieris brassicae*. J Comp Neurol 220:80–96.

1529 Safi K, Dechmann DKN. 2005. Adaptation of brain regions to habitat complexity: a
1530 comparative analysis in bats (Chiroptera). Proc Biol Sci 272:179–186.

1531 Salcedo C. 2011. Pollen preference for *Psychotria sp*. is not learned in the passion
1532 flower butterfly, *Heliconius erato*. J Insect Sci 11:25.

1533 Schildberger K. 1983. Local interneurons associated with the mushroom bodies and
1534 the central body in the brain of *Acheta domesticus*. Cell Tissue Res 230:573–
1535 586.

1536 Schoonhoven LM. 1968. Chemosensory Bases of Host Plant Selection. Annu Rev
1537 Entomol 13:115–136.

1538 Schürmann FW. 1970. Structure of the mushroom bodies of the insect brain. I.
1539 Synapses in the peduncle. Zeitschrift für Zellforsch und mikroskopische Anat
1540 (Vienna, Austria 1948) 103:365.

1541 Seymoure B, McMillan WO, Rutowski RL. Corneal area and facet diameters in
1542 Longwing (*Heliconius*) butterflies vary with body size and sex but not light
1543 environment nor mimicry ring. *in review.*

1544 Shumway CA. 2008. Habitat complexity, brain, and behavior. Brain Behav Evol
1545 72:123–134.

1546 Silva AK, Gonçalves GL, Moreira GRP. 2014. Larval feeding choices in heliconians:
1547 Induced preferences are not constrained by performance and host plant
1548 phylogeny. Anim Behav 89:155–162.

1549 Sivinski J. 1989. Mushroom body development in nymphalid butterflies: A correlate
1550 of learning? J Insect Behav 2:277–283.

1551 Sjöholm M, Sinakevitch I, Ignell R, Strausfeld NJ, Hansson BS. 2005. Organization
1552 of Kenyon cells in subdivisions of the mushroom bodies of a lepidopteran insect.
1553 J Comp Neurol 491:290–304.

1554 Skiri HT, Rø H, Berg BG, Mustaparta H. 2005. Consistent organization of glomeruli
1555 in the antennal lobes of related species of Heliothine moths. J Comp Neurol
1556 491:367–80.

1557 Smiley JT. 1978. The host plant ecology of *Heliconius* butterflies in northeastern
1558 Costa Rica. PhD. University of Texas at Austin, Austin, Texas.

1559 Smith AR, Seid MA, Jiménez LC, Wcislo WT. 2010. Socially induced brain
1560 development in a facultatively eusocial sweat bee *Megalopta genalis*
1561 (Halictidae). Proc Biol Sci 277:2157–2163.

1562 Snell-Rood EC, Davidowitz G, Papaj DR. 2011. Reproductive tradeoffs of learning in
1563 a butterfly. Behav Ecol 22:291–302.

1564 Snell-Rood EC, Papaj DR, Gronenberg W. 2009. Brain size: a global or induced cost
1565 of learning? Brain Behav Evol 73:111–28.

1566 Snell-Rood EC. 2013. An overview of the evolutionary causes and consequences of
1567 behavioural plasticity. Anim Behav 85:1004–1011.

1568 Stopfer M. 2014. ScienceDirect Central processing in the mushroom bodies. Curr
1569 Opin Insect Sci 6:99–103. A

1570 Tamura K, Peterson D, Peterson N, Stecher G, Nei M, Kumar S. 2011. MEGA5:
1571 molecular evolutionary genetics analysis using maximum likelihood,
1572 evolutionary distance, and maximum parsimony methods. Mol Biol Evol
1573 28:2731–9.

1574 R Development Consortium. 2008. R: A language and environment for statistical
1575 computing. R Foundation for Statistical Computing, Vienna, Austria. ISBN 3-
1576 900051-07-0. URL http//wwwR-project.org.

1577 Trautwein MD, Wiegmann BM, Beutel R, Kjer KM, Yeates DK. 2012. Advances in
1578 insect phylogeny at the dawn of the postgenomic era. Annu Rev Entomol
1579 57:449–468.

1580 Turner JRG. 1971. Experiments on the demography of tropical butterflies. II.
1581 Longevity and home-range behaviour in *Heliconius erato*. Biotropica 3:21–31.

1582 Turner JRG. 1981. Adaptation and evolution in *Heliconius*: A defense of
1583 NeoDarwinism. Annu Rev Ecol Syst 12:99–121.

1584 Warren AD, Davis KJ, Strangeland EM, Pelham JP, Grishin NV. 2013. Illustrated
1585 lists of American butterflies. http://butterfliesofamerica.com

1586 Warton DI, Duursma RA., Falster DS, Taskinen S. 2012. smatr 3- an R package for
1587 estimation and inference about allometric lines. Methods Ecol Evol 3:257–259.

1588 Wei H, el Jundi B, Homberg U, Stengl M. 2010. Implementation of pigment-
1589 dispersing factor-immunoreactive neurons in a standardized atlas of the brain of
1590 the cockroach *Leucophaea maderae*. J Comp Neurol 518:4113–33.

1591 Whiting BA, Barton RA. 2003. The evolution of the cortico-cerebellar complex in
1592 primates: Anatomical connections predict patterns of correlated evolution. J
1593 Hum Evol 44:3–10.

1594 Withers G, Day NF, Talbot EF, Dobson HEM, Wallace CS. 2008. Experience-
1595 dependent plasticity in the mushroom bodies of the solitary bee *Osmia lignaria*
1596 (Megachilidae). Dev Neurobiol 68:73–82.

1597 Withers GS, Fahrbach SE, Robinson GE. 1993. Selective neuroanatomical plasticity
1598 and division of labour in the honeybee. Nature364:238–40.

1599 Zars T. 2000. Behavioral functions of the insect mushroom bodies. Curr Opin
1600 Neurobiol 10:790–795.

1601

1602 ## Abbreviations

AL	antennal lobe
aMe	accessory medulla
AN	antennal nerve
AOTu	anterior optic tubercule
CB	central body
CBL	lower central body
CBU	upper central body
CFN	central fibrous neuropil of *AL*
DMSO	dimethyl suphoxide
Glom	glomeruli
HBS	HEPES-buffered saline
iMe	inner medulla
iRim	inner rim of the lamina
La	lamina
LAL	lateral accessory lobes
Lo	lobula
LoP	lobula plate
LU	lower unit of *AOTu*
MB	mushroom body
MB-ca	mushroom body calyx
MB-lo	mushroom body lobes
MB-pe	mushroom body peduncle
MB-lo+pe	mushroom body lobes and peduncle combined
MBr	midbrain
Me	medulla
MGC	macro-glomeruli complex
NGS	normal goat serum
no	noduli
NU	nodule unit of *AOTu*
oMe	outer medulla
OR	olfactory receptor
OGC	optic glomerular complex
PA	pyrrolizidine alkaloids
PB	protocerebral bridge
PC	principal component
POTu	posterior optic tubercle
rMid	rest of midbrain
SP	strap of *AOTu*
UU	upper unit of *AOTu*
ZnFA	Zinc-Formaldehyde solution

1603

1604

Figure Legends

Figure 1: Overview of the anatomy of the *Heliconius* brain.

3D models of *H. erato* (**A–G**) and *H. hecale* (**A'–G'**). **B–D** and **B'–D':** Volume rendering of synapsin immunofluorescence showing the surface morphology of the brain neuropil from the anterior (A/A'), posterior (B/B'), and dorsal (C/C') view. **E–G** and **E'–G':** Surface reconstructions of the major neuropil compartments from the anterior (D), posterior (E), and dorsal (F) view. Neuropil in yellow-orange: visual neuropil, green: central complex, blue: antennal lobes, red: mushroom bodies. See Figures 2–4 for further anatomical detail. The individuals displayed are male. Images in A/A' are from Warren et al. (2013). Scale bars = 25 mm in A/A'; 500 µm in B–D/B'–D'.

Figure 2: Anatomy of the sensory neuropils.

Images A–H are from male *H. hecale.* **A:** Surface reconstructions of the optic lobe neuropils viewed from anterior (left image) and posterior (right image). They comprise the lamina (La), the medulla (Me), and accessory medulla (aMe), the lobula (Lo), the lobula plate (LoP) and the optic glomerulus (OG). **B:** Surface reconstruction of the optic glomerulus (OG) viewed along the anterior-posterior axis (top) and an anterior view (bottom)**. C:** Surface reconstruction of the anteriot optic tubercle (AOTu)**. D–J:** Synapsin immunofluorescence in single confocal sections of the optic lobe of *H. hecale*. **D:** Horizontal section showing all four major optic lobe neuropils (La, Me, Lo, LoP). **E:** Frontal section showing the inner rim (iRim) of the lamina, a thin layer on its inner surface that is defined by intense synapsin immunofluorescence. Synapsin immunostaining also reveals the laminated structure of the medulla with two main subdivisions, the outer and inner medulla (oMe, iMe). **F:** The OG is located medially to the Lo; frontal section, the midbrain (MBr) occupies the left half of the frame. **G,H:** Frontal sections showing a small, irregular neuropil (ir) observed running from the anterior-ventral boundary of the aME as in *D. plexippus* (Heinze and Reppert, 2012).

Figure 3: Anatomy of the antennal lobe

A: 3D reconstruction of individual antennal lobe (AL) glomeruli superimposed on a volume rendering of the anterior surface of the midbrain. **B:** Synapsin immunofluorescence in a single frontal confocal section showing the glomeruli (Glom) surrounding the central fibrous neuropil (CFN). Images A–B are from male *H. hecale*. **C,D:** Allometric grade-shifts between Glom (circles) or CFN (triangles) volume and unsegmented midbrain volume (C), and between Glom and CFN volume (D) in *G. zavaleta* (solid blue), *H. erato* (black filled with red) and *H. hecale* (orange filled with yellow). Scale bars = 500 µm in A; 50 µm in B,C,G,H; 100 µm in B–F, J; 200 µm in I.

Figure 4: Anatomy of the central complex

A/A': Surface reconstruction of the central complex from an anterolateral (A) and oblique posteroventral (A') view, showing the upper and lower subunit of the central body (CBU, CBL), the noduli (No), the protocerebral bridge (PB) and posterior optic tubercles (POTu). **B–G:** Synapsin immunofluorescence in single confocal sections. **B:** Horizontal section showing the upper and lower subunit of the CB in relation to the antennal lobes (AL) and the calyx (MB-ca) and pedunculus (MB-pe) of the mushroom body. **C,D:** Frontal confocal sections at the level of the CBL (C) and CBU (D); the CB subunits are flanked by the profiles of the vertically running MB-pe on either side. **E:** Frontal section showing the location of the PB ventrally to the MB-ca. **F:** POTu positioned ventrally to the MB-ca in a frontal section. **G:** Frontal section showing position of the paired No ventrally to CBL and CBU. All images are from a male *H. hecale*. Scale bars = 100 µm in B–D, G; 50 µm in E,F.

Figure 5: Anatomy of the mushroom body

A–C: Surface reconstruction of the mushroom body viewed (A), orthogonal to the anterior-posterior axis from a medial vantage point level with the peduncle; (B), from anterior; and (C), from posterior. The main components are the calyx (MB-ca) shown in dark red, and the peduncule (MB-pe) and lobes (MB-lo) shown in bright red. A Y-tract, shown in magenta, runs parallel and slightly medial to the MB-pe. **D–K:** Synapsin immunofluorescence in individual confocal sections. **D:** anterior view of the midbrain showing the MB-lo, an asterik indicates the probably ventral lobe, otherwise the individual lobes and loblets of the MB-lo are fused. **E:** Frontal section at a

posterior level near the end of the MB-pe, showing the profiles of the MB-ca with its zonation into an outer and a medial ring. **F,G** and **J,K**: Horizontal confocal sections through the midbrain at increasing depths from dorsal towards ventral, showing MB structure in relation to neighboring neuropil: the anterior optic tubercle (AOTu in F,G); the antennal lobe (AL in G,J); and the central body upper division (CBU in K). **H:** An example of a female *H. erato* where the MB-ca is deformed due expansion into the optic lobe and constriction (C) at the optic stalk by the neural sheath surrounding the brain. **I:** Pitted surface of the MB-ca in a very posterior tangential horizontal section. The pitting is related to what appear to be columnar domains within the calyx neuropil (*cf.* MB-ca in J,K,M). **L:** Areas of intense synapsin staining in the optic stalk (OS*); Lo, lobula; OG, optic glomerulus. **M:** Frontal section near the base of the calyx (MB-ca) showing a satellite neuropil (sat.) located near to the MB-pe. **N:** A Y-tract runs parallel with, and dorsally and slightly medially to the MB-pe; both are seen in profile in this frontal section. **O:** A fiber bundle (fb) connected to the AOTu running near the junction between the MB-pe and MB-lo. With the exception of I, all images are from a male *H. hecale.* Scale bars A-G, J-K = 200 µm, H-I, L-O = 100 µm.

Figure 6: Age and environment dependent growth of the mushroom bodies

Surface reconstruction of the mushroom body viewed along the anterior-posterior axis for wild-caught, old and young insectary-reared individuals of *H. erato* (**A**) and *H. hecale* (**A'**). Representative individuals were chosen as those closest to the group mean volume. Scale bar = 200 µm. **B-C/B'-C':** allometric relationships between MB-lo+pe (B/B'), or MB-ca (C/C'),and the volume of the unsegmented midbrain (rMid) for *H. erato* (B/C) and *H. hecale* (B'/C'). Data for wild caught individuals are in green, data for old insectary-reared individuals in dark blue, and data for young insectary-reared individuals are in light blue. Allometric slopes for each group are shown, the slope, intercepts and major-axis means are compared in Table 2, 3.

Figure 7: Age and environment dependent growth of brain components

A,D: Comparisons of raw volumes of total neuropil, total OL neuropil, total midbrain neuropil between wild-caught, old and young insectary-reared individuals of *H. erato* (A) and *H. hecale* (D). Significance of pair-wise comparisons are shown along the x-axis (young-old = orange; old-wild = dark red; n.s. = $p>0.05$, * = $p<0.05$, ** = $p<0.01$, *** = $p < 0.001$). **B:** Allometric scaling of LoP in *H. erato*. **C:** Allometric

scaling of PB in *H. erato*. **E:** Allometric scaling of OG in *H. hecale*. **F:** Allometric scaling of CB in *H. hecale*. Note in E and F the shifts in allometry occur along the x-axis, this is explained by the large difference in unsegmented midbrain volume observed between wild-caught and old insectary-reared individuals in *H. hecale* as displayed in D.

Figure 8: Divergence in brain structure between *H. erato* and *H. hecale.*

A–C: Species differences in brain-body scaling between *H. erato* (red) and *H. hecale* (orange). Grade-shifts towards larger neuropil volume relative to body length are seen for total neuropil (A) but are mainly driven by OL neuropil (B) rather than midbrain neuropil (C). **D:** Discriminant Function analysis of segmented neuropil volumes and the unsegmented midbrain volume separates wild individuals of the two species along a single axis (yellow, orange ring: wild *H. hecale;* red, black ring: wild *H. erato*). **E, F:** DFA including wild and old insectary-reared individuals of both species (solid orange = old insectary-reared *H. hecale*; solid black: old insectary-reared *H. erato*). E displays DF1 vs. DF2 to illustrate that DF1 accounts for the most variation between species, F displays DF2 vs. DF3 to illustrate that these axes separate wild and old insectary-reared individuals of the same species.

Figure 9: Divergence in brain structure across Lepidoptera, and in mushroom body size across insects.

A: Phylogenetic relationships of Lepidoptera (red branches) and other insects (grey branches) for which comparable data are available. Branches are not drawn proportional to divergence dates, numbers refer to labels in panel E. **B,C:** Principal Component analysis of segmented neuropil volumes, corrected for allometric scaling with the unsegmented midbrain and phylogeny. **B:** Analysis using all neuropil. **C:** Analysis excluding the optic lobe neuropil. Species data points are indicated by the first letter of their genus and species name: *D.p = Danaus plexippus*; *H.e = Heliconius erato*; *H.h = H. hecale*; *G.z = Godyris zavaleta*; *H.v = Heliothis virescens*; *M.s = Manduca sexta*. **D:** The proportion of the midbrain occupied by MB-ca (dark red) and MB-lo+pe (light red) in four butterflies, and two other insects with fully comparable data. **E:** Across a wider sample of insects (shown in A), when expressed as a percentage of total volume of OL, AL, CB and MB, *Apis mellifera* (solid blue) and *Heliconius* (solid red) stand out as having expanded mushroom bodies, correcting for

1740 the size of the optic neuropil, compared to other Lepidoptera (unfilled red circles) and
1741 other insects (unfilled blue circles). The line was fitted by PGLS. All insect images in
1742 A are from Wikimedia commons and were released under the Creative Commons
1743 License, except *Heliconius* (see Fig. 1).
1744
1745
1746
1747
1748
1749
1750
1751
1752
1753
1754
1755
1756
1757
1758
1759
1760
1761
1762
1763
1764
1765
1766
1767
1768
1769

Tables

Table 1: Neuropil volumes and body size of A) *H. erato* and B) *H. hecale*

Table 2: Comparisons between old (O) and young (Y) insectary-reared individuals for A) *H. erato* and B) *H. hecale*. *r* is the effect size. DI indicates the group with a higher value of α, β or fitted axis mean.

Table 3: Comparisons between wild caught (W) and old insectary-reared individuals for A) *H. erato* and B) *H. hecale*. *r* is the effect size. DI indicates the group with a higher value of α, β or fitted axis mean.

Table 4: Comparisons between *H. erato* and *H. hecale* for A) wild caught and B) old insectary-reared individuals. *r* is the effect size. DI indicates the species with a higher value of α, β or fitted axis mean.

Table 5: Discriminant function analysis of variation between wild and old insectary-reared *H. erato* and *H. hecale*. A) Canonical discrimant function coefficitions for DF1-3. B) Disrciminant function statistics. C) Results of a MANOVA of DF1-3 to test for associations with species, group, and species-group interactions.

Table 6: Loadings on Principal Components Analysis of the relative size of brain components across six Lepidoptera.

Table 1

A) *H. erato*

	wild caught				*old insectary reared*		*young insectary reared*	
	mean (*n* = 10)	**SD**	**Rel. SD (%)**	**% total Neuropil**	**mean (*n* = 10)**	**SD**	**mean (*n* = 10)**	**SD**
Body mass (g)	0.093	0.017	19.999	-	0.074	0.014	0.088	0.019
Body length (mm)	23.833	1.426	5.983	-	23.095	1.773	22.671	0.951
Wing span (mm)	71.408	3.278	4.591	-	69.744	4.12	68.786	2.55
Lamina	7.409E+07	1.052E+07	14.192	13.459	6.95E+07	1.61E+07	5.49E+07	1.25E+07
Medulla	2.396E+08	3.617E+07	15.094	43.523	2.45E+08	2.76E+07	1.90E+08	3.32E+07
Accessory medulla	1.633E+05	3.609E+04	22.094	0.030	1.59E+05	4.61E+04	9.77E+04	1.93E+04
Inner lobula	2.630E+07	4.203E+06	15.984	4.777	2.79E+07	2.89E+06	2.07E+07	4.32E+06
Lobula plate	1.393E+07	2.083E+06	14.952	2.531	1.35E+07	2.22E+06	1.04E+07	2.07E+06
OG	1.054E+06	2.400E+05	22.769	0.191	1.05E+06	2.42E+05	8.85E+05	2.26E+05
Antennal lobes	1.185E+07	2.450E+06	20.671	2.153	1.19E+07	2.49E+06	7.72E+06	1.10E+06
AOTu	2.199E+06	4.535E+05	20.618	0.400	2.26E+06	3.28E+05	1.52E+06	3.27E+05
MB calyx	4.672E+07	9.290E+06	19.886	8.486	4.50E+07	1.22E+07	2.79E+07	5.75E+06
MB peduncle	6.043E+06	1.109E+06	18.343	1.098	6.15E+06	1.35E+06	5.57E+06	1.58E+06
MB lobes	2.267E+07	5.812E+06	25.641	4.118	2.17E+07	4.26E+06	1.28E+07	2.31E+06
Central body lower	3.017E+05	5.189E+04	17.198	0.055	2.83E+05	6.00E+04	2.24E+05	3.81E+04
Central body upper	1.180E+06	1.788E+05	15.153	0.214	1.17E+06	2.57E+05	8.90E+05	1.36E+05
Noduli	2.966E+04	1.146E+04	38.631	0.005	3.09E+04	1.64E+04	3.16E+04	8.46E+03
Protocerebral bridge	2.120E+05	4.804E+04	22.658	0.039	1.96E+05	5.04E+04	1.39E+05	2.02E+04
POTu	4.213E+04	9.976E+03	23.681	0.008	4.20E+04	1.43E+04	2.73E+04	7.93E+03
Total midbrain	1.954E+08	3.365E+07	17.222	35.490	2.04E+08	2.70E+07	1.39E+08	2.28E+07

Table 1 continued
B) *H. hecale*

	wild caught				*old insectary reared*		*young insectary reared*	
	mean (*n* = 10)	**SD**	**Rel. SD (%)**	**% total Neuropil**	**mean (*n* = 9)**	**SD**	**mean (*n* = 10)**	**SD**
Body mass (g)	0.163	0.025	15.317	-	0.154	0.046	0.171	0.047
Body length (mm)	29.693	3.097	10.431	-	28.189	3.0631	29.206	2.75
Wing span (mm)	88.129	8.004	9.082	-	80.6	7.134	86.34	8.012
Lamina	9.751E+07	1.826E+07	18.721	13.939	9.39E+07	2.17E+07	9.64E+07	1.50E+07
Medulla	2.986E+08	5.342E+07	17.888	42.689	2.48E+08	3.81E+07	2.42E+08	3.66E+07
Accessory medulla	1.660E+05	2.951E+04	17.782	0.024	1.40E+05	2.80E+04	1.38E+05	3.67E+04
Inner lobula	3.056E+07	5.630E+06	18.422	4.369	2.80E+07	4.64E+06	2.45E+07	5.06E+06
Lobula plate	1.648E+07	2.972E+06	18.031	2.356	1.45E+07	2.45E+06	1.27E+07	2.53E+06
OG	1.099E+06	3.396E+05	30.894	0.157	9.93E+05	2.12E+05	9.24E+05	2.10E+05
Antennal lobes	1.216E+07	2.056E+06	16.905	1.739	1.09E+07	1.34E+06	9.36E+06	1.59E+06
AOTu	2.572E+06	6.144E+05	23.891	0.368	2.30E+06	4.46E+05	2.02E+06	3.76E+05
MB calyx	5.271E+07	1.611E+07	30.569	7.534	3.60E+07	7.49E+06	2.60E+07	7.48E+06
MB peduncle	6.680E+06	1.525E+06	22.834	0.955	5.92E+06	1.30E+06	4.91E+06	1.39E+06
MB lobes	2.421E+07	6.279E+06	25.930	3.461	1.79E+07	3.56E+06	1.32E+07	3.51E+06
Central body lower	3.109E+05	6.362E+04	20.467	0.044	2.91E+05	7.15E+04	2.47E+05	3.74E+04
Central body upper	1.093E+06	2.026E+05	18.541	0.156	1.16E+06	2.05E+05	9.65E+05	1.79E+05
Noduli	4.207E+04	1.713E+04	40.730	0.006	3.34E+04	8.35E+03	3.06E+04	1.28E+04
Protocerebral bridge	2.424E+05	5.657E+04	23.335	0.035	2.00E+05	3.09E+04	1.64E+05	1.75E+04
POTu	4.183E+04	1.257E+04	30.057	0.006	3.74E+04	8.47E+03	3.20E+04	8.27E+03
Total midbrain	2.551E+08	6.253E+07	24.513	36.465	1.82E+08	2.28E+07	1.50E+08	2.25E+07

Table 2

A) *H. erato*

	Volume			Scaling coefficient (β)			Intercept (α)			Major Axis Shift		
	t17	**p**	**r (DI)**	**Likelihood Ratio**	**p**	**r (DI)**	**Wald χ2**	**p**	**r (DI)**	**Wald χ2**	**p**	**r (DI)**
Lamina	2.432	0.026	0.508 (O)	2.019	0.155	-	2.895	0.089	-	13.196	0.000	0.833 (O)
Medulla	4.118	0.001	0.707 (O)	0.090	0.765	-	1.127	0.288	-	19.405	0.000	1.000 (O)
Accessory medulla	3.802	0.001	0.678 (O)	3.976	0.046	0.458 (O)	-	-	-	-	-	-
Inner lobula	4.173	0.001	0.711 (O)	0.246	0.620	-	1.587	0.208	-	20.284	0.000	1.000 (O)
Lobula plate	3.266	0.005	0.621 (O)	0.523	0.470	-	3.802	0.051	-	19.034	0.000	1.000 (O)
OG	1.412	0.176	-	0.385	0.535	-	5.694	0.017	0.547 (Y)	10.622	0.001	0.748 (O)
Antennal lobes	5.080	0.000	0.776 (O)	4.169	0.041	-	0.214	0.644	-	27.584	0.000	1.000 (O)
AOT	5.192	0.000	0.783 (O)	0.109	0.741	-	0.123	0.726	-	26.321	0.000	1.000 (O)
MB calyx	4.050	0.001	0.701 (O)	3.679	0.055	-	1.607	0.205	-	19.177	0.000	1.000 (O)
MB lobes+peduncle	4.806	0.000	0.759 (O)	0.963	0.326	-	0.373	0.541	-	23.250	0.000	1.000 (O)
CB L+U	3.272	0.004	0.622 (O)	2.364	0.124	-	1.807	0.179	-	16.530	0.000	0.933 (O)
Protocerebral bridge	3.169	0.006	0.609 (O)	5.996	0.014	0.562 (O)	-	-	-	-	-	-
POTu	2.772	0.013	0.558 (O)	1.539	0.215	-	4.124	0.042	0.466 (Y)	14.953	0.000	0.887 (O)
Total Mid	4.192	0.001	0.713 (O)	-	-	-	-	-	-	-	-	-
rMid	5.771	0.000	0.814 (O)	-	-	-	-	-	-	-	-	-
Total OL	5.076	0.000	0.776 (O)	-	-	-	-	-	-	-	-	-
Total neuropil	5.153	0.000	0.781 (O)	-	-	-	-	-	-	-	-	-

B) *H. hecale*

	Volume			Scaling coefficient (β)			Intercept (α)			Major Axis Shift		
	t18	**p**	**r (DI)**	**Likelihood Ratio**	**p**	**r (DI)**	**Wald χ2**	**p**	**r (DI)**	**Wald χ2**	**p**	**r (DI)**
Lamina	-0.424	0.677	-	1.866	0.172	-	11.902	0.001	0.771 (Y)	1.043	0.307	-
Medulla	0.333	0.743	-	0.494	0.482	-	21.674	0.000	1.000 (Y)	1.971	0.160	-
Accessory medulla	0.238	0.814	-	0.094	0.759	-	3.044	0.081	-	3.088	0.079	-
Inner lobula	1.538	0.141	-	0.002	0.961	-	3.544	0.060	-	4.501	0.034	0.474 (O)
Lobula plate	1.683	0.110	-	0.066	0.797	-	1.577	0.209	-	5.031	0.025	0.502 (O)
OG	0.617	0.545	-	0.266	0.606	-	4.408	0.036	0.470 (Y)	3.045	0.081	-
Antennal lobes	2.418	0.026	-	1.795	0.180	-	2.396	0.122	-	6.451	0.011	0.570 (O)
AOT	1.496	0.152	-	0.101	0.751	-	2.166	0.141	-	4.656	0.031	0.483 (O)
MB calyx	3.177	0.005	0.599 (O)	0.283	0.595	-	0.104	0.747	-	9.166	0.002	0.677 (O)
MB lobes+peduncle	2.707	0.014	0.538 (O)	0.147	0.702	-	0.015	0.902	-	7.594	0.006	0.616 (O)
CB L+U	2.218	0.040	0.463 (O)	3.291	0.070	-	0.859	0.354	-	7.221	0.007	0.601 (O)
Protocerebral bridge	3.291	0.004	0.613 (O)	1.043	0.307	-	0.172	0.678	-	9.448	0.002	0.687 (O)
POTu	1.494	0.153	-	0.078	0.780	-	0.736	0.391	-	6.292	0.012	0.561 (O)
Total Mid	3.054	0.007	0.584 (O)	-	-	-	-	-	-	-	-	-
rMid	2.854	0.011	0.558 (O)	-	-	-	-	-	-	-	-	-
Total OL	0.280	0.783	-	-	-	-	-	-	-	-	-	-
Total neuropil	1.082	0.293	-	-	-	-	-	-	-	-	-	-

Table 3

A) *H. erato*

	Volume			Scaling coefficient (β)			Intercept (α)			Major Axis Shift		
	t17	**p**	**r (DI)**	**Likelihood Ratio**	**p**	**r (DI)**	**Wald χ2**	**p**	**r (DI)**	**Wald χ2**	**p**	**r (DI)**
Lamina	0.892	0.385	-	3.685	0.055	-	3.605	0.058	-	0.210	0.646	-
Medulla	-0.426	0.676	-	0.269	0.604	-	2.056	0.152	-	1.269	0.260	-
Accessory medulla	0.359	0.724	-	5.150	0.023	0.521 (O)	-	-	-	-	-	-
Inner lobula	-1.056	0.306	-	0.283	0.595	-	1.004	0.316	-	1.999	0.157	-
Lobula plate	0.430	0.673	-	4.963	0.026	0.511 (O)	-	-	-	-	-	-
OG	0.116	0.909	-	2.148	0.143	-	2.055	0.152	-	0.848	0.357	-
Antennal lobes	-0.035	0.972	-	1.695	0.193	-	2.269	0.132	-	0.899	0.343	-
AOT	-0.490	0.631	-	0.483	0.487	-	1.318	0.251	-	1.456	0.227	-
MB calyx	0.511	0.616	-	5.833	0.016	0.554 (O)	-	-	-	-	-	-
MB lobes+peduncle	0.239	0.814	-	0.714	0.398	-	4.418	0.036	0.482 (W)	7.594	0.006	0.632 (W)
CB L+U	0.394	0.699	-	4.272	0.039	0.474 (O)	-	-	-	-	-	-
Protocerebral bridge	0.845	0.410	-	4.413	0.036	0.482 (O)	-	-	-	-	-	-
POTu	0.196	0.847	-	3.726	0.054	-	2.730	0.098	-	0.905	0.341	-
Total Mid	-0.732	0.474	-	-	-	-	-	-	-	-	-	-
rMid	-1.787	0.092	-	-	-	-	-	-	-	-	-	-
Total OL	-0.123	0.904	-	-	-	-	-	-	-	-	-	-
Total neuropil	-0.432	0.671	-	-	-	-	-	-	-	-	-	-

B) *H. hecale*

	Volume			Scaling coefficient (β)			Intercept (α)			Major Axis Shift		
	t18	**p**	**r (DI)**	**Likelihood Ratio**	**p**	**r (DI)**	**Wald χ2**	**p**	**r (DI)**	**Wald χ2**	**p**	**r (DI)**
Lamina	0.437	0.667	-	6.725	0.010	0.580 (O)	-	-	-	-	-	-
Medulla	2.293	0.034	0.475 (W)	9.165	0.002	0.677 (O)	-	-	-	-	-	-
Accessory medulla	1.898	0.074	-	3.728	0.054	-	1.463	0.227	-	8.056	0.005	0.688 (W)
Inner lobula	1.017	0.322	-	9.760	0.002	0.699 (O)	-	-	-	-	-	-
Lobula plate	1.609	0.125	-	6.081	0.014	0.551 (O)	-	-	-	-	-	-
OG	0.614	0.547	-	4.262	0.039	0.462 (O)	-	-	-	-	-	-
Antennal lobes	1.519	0.146	-	7.095	0.008	0.596 (O)	-	-	-	-	-	-
AOT	1.088	0.291	-	3.938	0.047	0.444 (O)	-	-	-	-	-	-
MB calyx	3.126	0.006	0.593 (W)	1.657	0.198	-	0.395	0.530	-	10.432	0.001	0.722 (W)
MB lobes+peduncle	2.536	0.021	0.513 (W)	3.759	0.053	-	1.603	0.205	-	8.811	0.003	0.664 (W)
CB L+U	-0.446	0.661	-	1.665	0.197	-	11.013	0.001	0.742 (O)	2.385	0.122	-
Protocerebral bridge	1.919	0.071	-	5.043	0.025	0.502 (O)	-	-	-	-	-	-
POTu	0.551	0.588	-	5.420	0.020	0.521 (O)	-	-	-	-	-	-
Total Mid	3.658	0.002	0.653 (W)	-	-	-	-	-	-	-	-	-
rMid	3.417	0.003	0.627 (W)	-	-	-	-	-	-	-	-	-
Total OL	1.728	0.101	-	-	-	-	-	-	-	-	-	-
Total neuropil	2.553	0.020	0.516 (W)	-	-	-	-	-	-	-	-	-

Table 4
A) Wild

	Volume			Scaling coefficient (β)			Intercept (α)			Major Axis Shift		
	t18	**p**	**r (DI)**	**Likelihood Ratio**	**p**	**r (DI)**	**Wald χ2**	**p**	**r (DI)**	**Wald χ2**	**p**	**r (DI)**
Lamina	3.268	0.004	0.610 (Hh)	0.072	0.789	-	0.095	0.758	-	11.283	0.001	0.751 (Hh)
Medulla	2.713	0.014	0.539 (Hh)	1.256	0.262	-	1.311	0.252	-	9.069	0.003	0.673 (Hh)
Accessory medulla	0.217	0.831	-	1.608	0.205	-	7.737	0.005	0.622 (He)	3.748	0.053	-
Inner lobula	1.817	0.086	-	0.998	0.318	-	4.759	0.029	0.488 (He)	6.704	0.010	0.579 (Hh)
Lobula plate	2.200	0.041	-	1.883	0.170	-	4.924	0.026	0.496 (He)	7.685	0.006	0.620 (Hh)
OG	0.136	0.893	-	0.021	0.886	-	16.729	0.000	0.915 (He)	3.203	0.074	-
Antennal lobes	0.390	0.701	-	7.367	0.007	0.607 (He)	-	-	-	-	-	-
AOT	1.550	0.139	-	1.227	0.268	-	9.657	0.002	0.695 (He)	6.117	0.013	0.553 (Hh)
MB calyx	0.863	0.400	-	0.000	0.995	-	5.405	0.020	0.520 (He)	4.798	0.028	0.490 (Hh)
MB lobes+peduncle	0.683	0.504	-	1.189	0.275	-	6.934	0.008	0.589 (He)	4.608	0.032	0.480 (Hh)
CB L+U	-0.866	0.398	-	0.164	0.686	-	9.685	0.002	0.696 (He)	2.260	0.133	-
Protocerebral bridge	1.262	0.223	-	2.869	0.090	-	1.436	0.231	-	6.571	0.010	0.573 (Hh)
POTu	-0.251	0.804	-	2.952	0.086	-	3.166	0.075	-	4.390	0.036	0.469 (Hh)
Total Mid	2.713	0.014	0.539 (Hh)	-	-	-	-	-	-	-	-	-
rMid	3.582	0.002	0.645 (Hh)	-	-	-	-	-	-	-	-	-
Total OL	2.866	0.010	0.560 (Hh)	-	-	-	-	-	-	-	-	-
Total neuropil	2.977	0.008	0.574 (Hh)	-	-	-	-	-	-	-	-	-

B) Old insectary-reared

	Volume			Scaling coefficient (β)			Intercept (α)			Major Axis Shift		
	t17	p	r (DI)	Likelihood Ratio	p	r (DI)	Wald $\chi 2$	p	r (DI)	Wald $\chi 2$	p	r (DI)
Lamina	2.949	0.009	0.582 (Hh)	0.015	0.902	-	14.433	0.000	0.872 (Hh)	0.488	0.485	-
Medulla	0.358	0.725	-	0.454	0.501	-	5.089	0.024	0.518 (Hh)	0.561	0.454	-
Accessory medulla	-0.395	0.697	-	1.634	0.201	-	0.167	0.683	-	1.679	0.195	-
Inner lobula	-0.480	0.637	-	1.886	0.170	-	4.099	0.043	-	0.548	0.459	-
Lobula plate	1.162	0.261	-	0.088	0.767	-	7.951	0.005	0.647 (Hh)	0.069	0.793	-
OG	-0.515	0.613	-	0.038	0.846	-	0.564	0.453	-	1.060	0.303	-
Antennal lobes	-1.329	0.201	-	2.557	0.110	-	0.001	0.974	-	1.155	0.283	-
AOT	0.064	0.950	-	0.133	0.715	-	1.112	0.292	-	0.621	0.431	-
MB calyx	-1.567	0.134	-	1.276	0.259	-	0.229	0.633	-	2.724	0.099	-
MB lobes+peduncle	-1.961	0.066	-	0.000	0.991	-	0.195	0.659	-	2.710	0.100	-
CB L+U	-0.378	0.710	-	1.751	0.186	-	3.937	0.047	0.455 (Hh)	0.151	0.698	-
Protocerebral bridge	-0.188	0.853	-	3.341	0.068	-	3.601	0.058	-	0.195	0.659	-
POTu	-0.429	0.673	-	1.532	0.216	-	0.372	0.542	-	1.329	0.249	-
Total Mid	-2.177	0.043	0.467 (He)	-	-	-	-	-	-	-	-	-
rMid	-1.391	0.181	-	-	-	-	-	-	-	-	-	-
Total OL	1.158	0.262	-	-	-	-	-	-	-	-	-	-
Total neuropil	0.145	0.886	-	-	-	-	-	-	-	-	-	-

Table 5

A) Canonical discriminant function coefficients

Neuropil	DF 1	DF 2	DF 3
rMid	1.716	0.892	-1.404
aME	-0.177	-0.190	0.093
ME	0.167	2.615	0.356
Lo	-1.906	-0.122	-0.802
LoP	0.000	-2.417	-0.287
OG	-0.224	-0.451	0.412
La	1.626	-0.517	0.591
AOTu	-0.570	-0.232	0.369
AL	-1.117	-0.565	0.296
MB-ca	-0.467	0.238	1.950
MB-lo+pe	-0.074	0.353	-0.935
CB	0.860	-0.619	-0.777
PB	0.755	0.741	0.726
POTu	-0.311	0.472	0.161

B) Discrimant function statistics

Correct group assignment		87%	
Eignevalue	3.090	2.065	0.528
% of variance	54.400	36.300	9.300
Wilks' Lambda	0.052	0.214	0.655
$\chi 2$	70.855	37.047	10.169
p	0.004	0.074	0.601

C) MANOVA statistics

F1(Species)	97.2632***	0.550	1.491
F1(Group)	4.6411*	11.695***	15.546***
F1(Species*Group)	0.000	38.172***	1.184

Table 6

A) Midbrain only

	Loadings	
	Residuals	
Neuropil	**PC1**	**PC2**
Antennal lobe	-0.981	-0.045
CB L+U	-0.798	0.406
MB Calyx	0.962	0.11
MB lobes+peduncle	0.952	0.231
AOTu	-0.047	0.966

B) Whole neuropil

	Loadings	
	Residuals	
Neuropil	**PC1**	**PC2**
Antennal lobe	0.761	0.619
CB L+U	0.671	0.67
MB Calyx	-0.961	0.212
MB lobes+peduncle	-0.942	0.222
AOTu	0.811	0.024
Medulla	0.042	-0.949
Lobula	0.92	-0.354
Lobula plate	0.962	-0.167

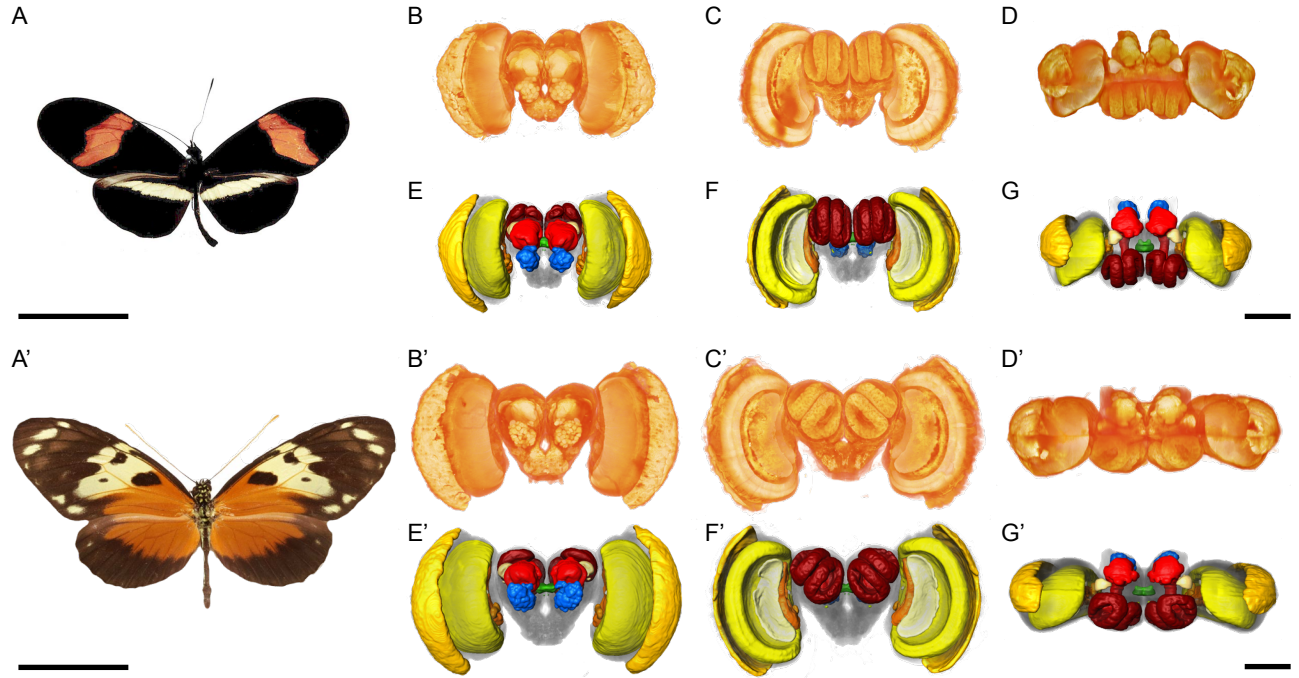
A
B
C
D
E
F
G
A'
B'
C'
D'
E'
F'
G'

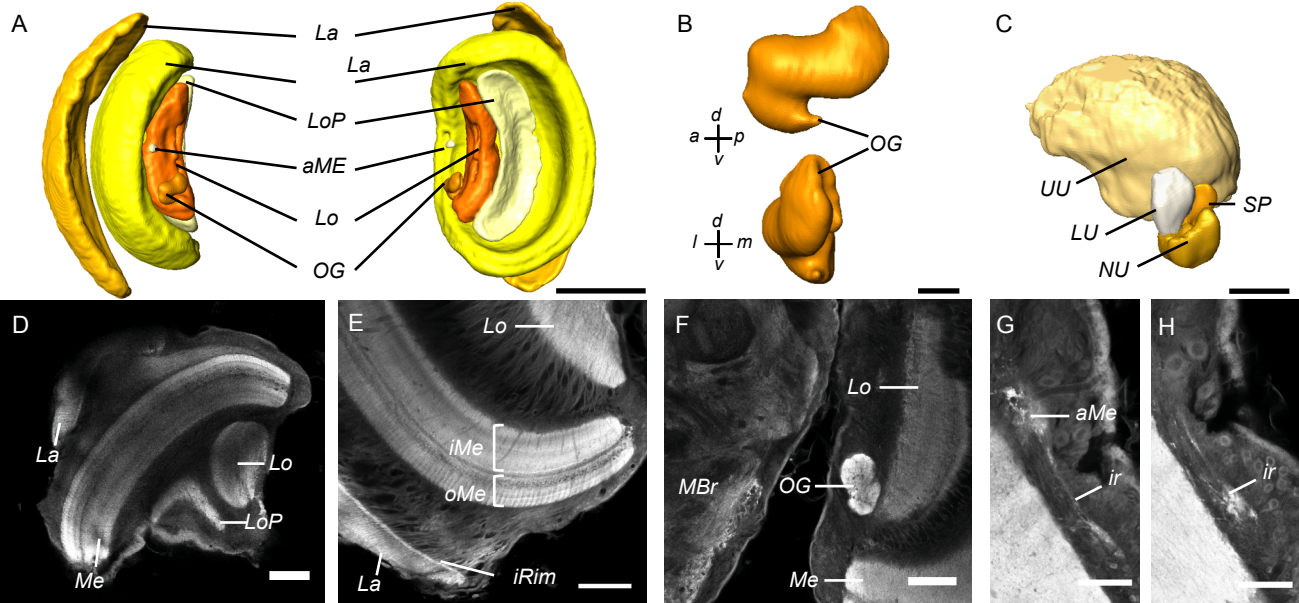
A
La
La
LoP
aME
Lo
OG
B
d
a
p
v
OG
d
l
m
v
C
UU
SP
LU
NU
D
La
Lo
LoP
Me
E
Lo
iMe
oMe
La
iRim
F
Lo
MBr
OG
Me
G
aMe
ir
H
ir

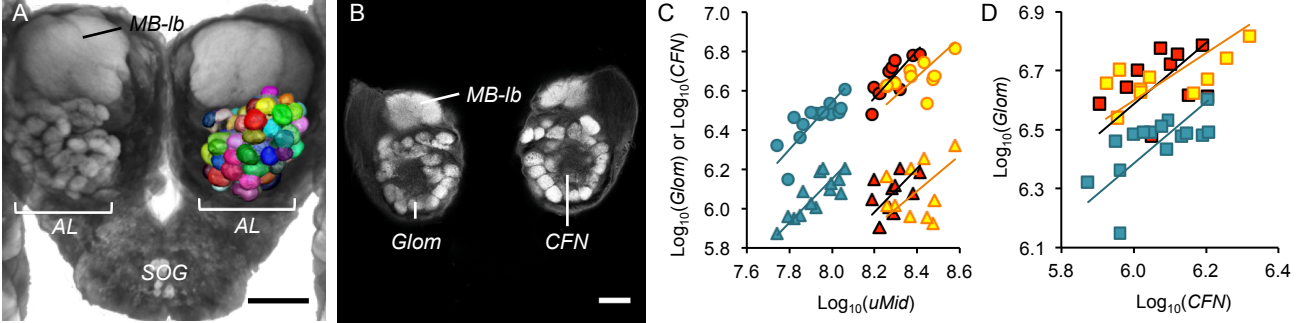
A
MB-lb
AL
AL
SOG
B
MB-lb
Glom
CFN
C
Log10(Glom) or Log10(CFN)
Log10(uMid)
D
Log10(Glom)
Log10(CFN)

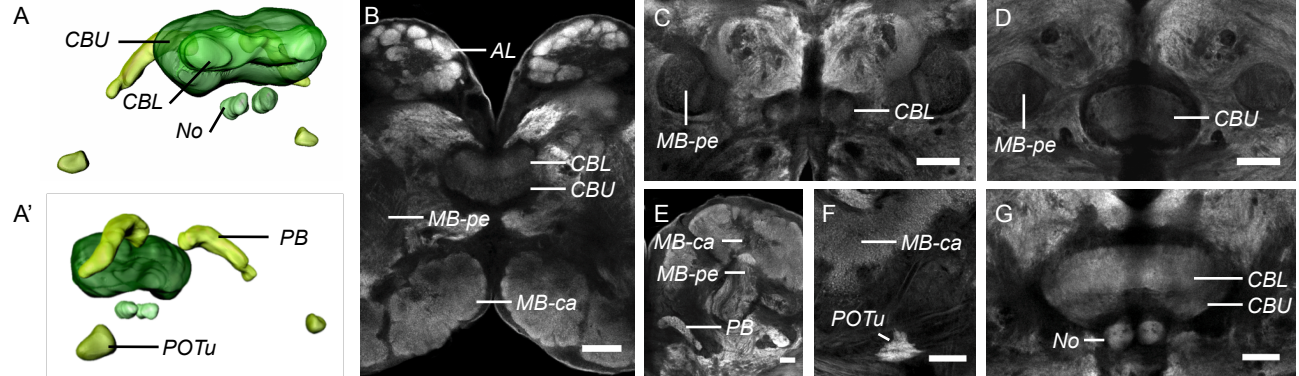
A
CBU
CBL
No
A'
PB
POTu
B
AL
CBL
CBU
MB-pe
MB-ca
C
CBL
MB-pe
D
CBU
MB-pe
E
MB-ca
MB-pe
PB
F
MB-ca
POTu
G
CBL
CBU
No

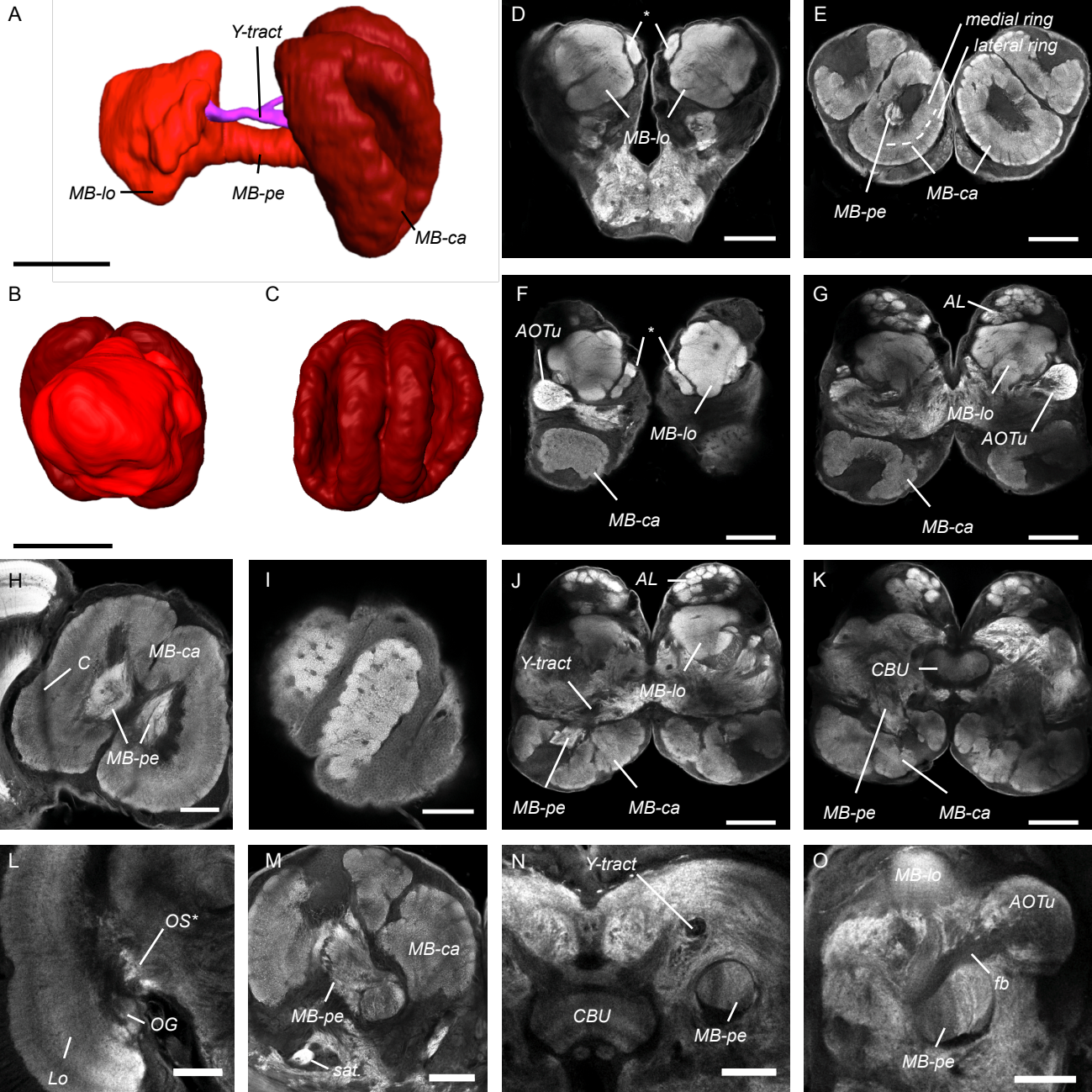
A
Y-tract
MB-lo
MB-pe
MB-ca
B
C
D
*
MB-lo
E
medial ring
lateral ring
MB-pe
MB-ca
F
AOTu
*
MB-lo
MB-ca
G
AL
MB-lo
AOTu
MB-ca
H
C
MB-ca
MB-pe
I
J
AL
Y-tract
MB-lo
MB-pe
MB-ca
K
CBU
MB-pe
MB-ca
L
OS*
OG
Lo
M
MB-ca
MB-pe
sat.
N
Y-tract
CBU
MB-pe
O
MB-lo
AOTu
fb
MB-pe

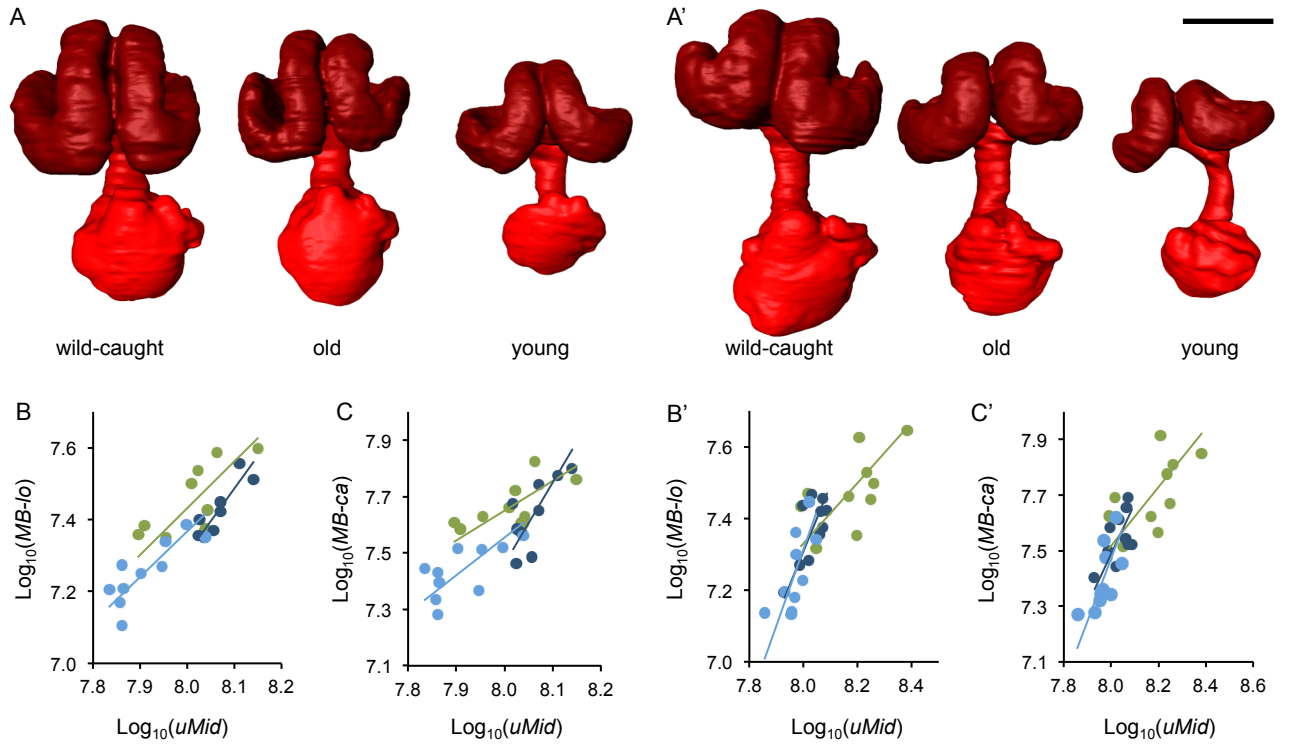
A
A'
wild-caught
old
young
wild-caught
old
young
B
C
B'
C'
Log10(MB-lo)
Log10(MB-ca)
Log10(uMid)
7.6
7.4
7.2
7.0
7.9
7.7
7.5
7.3
7.1
7.8
7.9
8.0
8.1
8.2
8.4
8.6

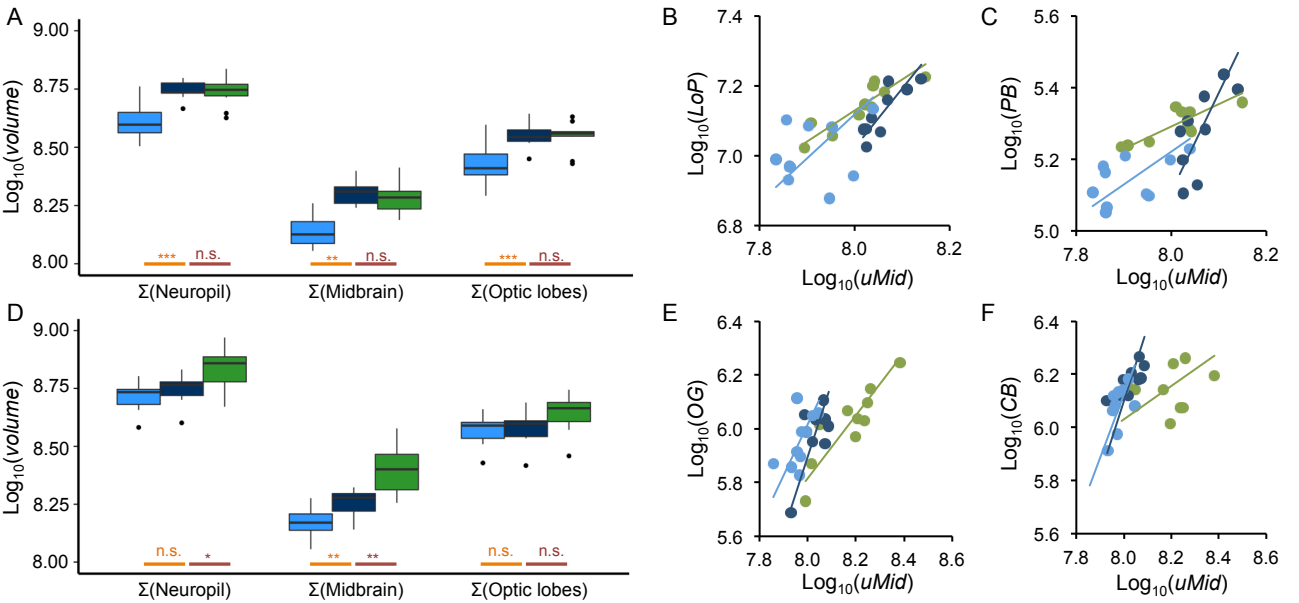
A
9.00
8.75
8.50
8.25
8.00
Log10(volume)
***
n.s.
**
n.s.
***
n.s.
Σ(Neuropil)
Σ(Midbrain)
Σ(Optic lobes)
D
9.00
8.75
8.50
8.25
8.00
Log10(volume)
n.s.
*
**
**
n.s.
n.s.
Σ(Neuropil)
Σ(Midbrain)
Σ(Optic lobes)
B
7.4
7.2
7.0
6.8
Log10(LoP)
7.8
8.0
8.2
Log10(uMid)
C
5.6
5.4
5.2
5.0
Log10(PB)
7.8
8.0
8.2
Log10(uMid)
E
6.4
6.2
6.0
5.8
5.6
Log10(OG)
7.8
8.0
8.2
8.4
8.6
Log10(uMid)
F
6.4
6.2
6.0
5.8
5.6
Log10(CB)
7.8
8.0
8.2
8.4
8.6
Log10(uMid)

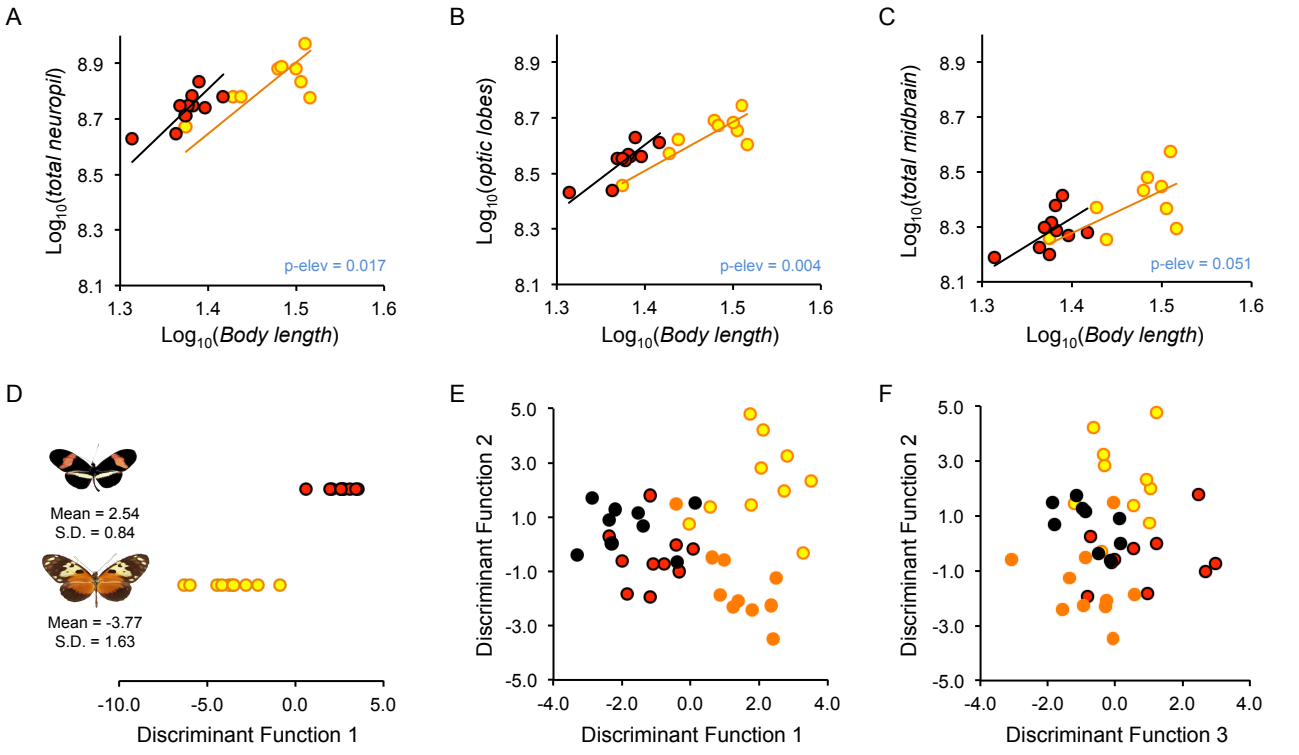
A
Log10(total neuropil)
8.9
8.7
8.5
8.3
8.1
1.3
1.4
1.5
1.6
Log10(Body length)
p-elev = 0.017
B
Log10(optic lobes)
8.9
8.7
8.5
8.3
8.1
1.3
1.4
1.5
1.6
Log10(Body length)
p-elev = 0.004
C
Log10(total midbrain)
8.9
8.7
8.5
8.3
8.1
1.3
1.4
1.5
1.6
Log10(Body length)
p-elev = 0.051
D
Mean = 2.54
S.D. = 0.84
Mean = -3.77
S.D. = 1.63
-10.0
-5.0
0.0
5.0
Discriminant Function 1
E
Discriminant Function 2
5.0
3.0
1.0
-1.0
-3.0
-5.0
-4.0
-2.0
0.0
2.0
4.0
Discriminant Function 1
F
Discriminant Function 2
5.0
3.0
1.0
-1.0
-3.0
-5.0
-4.0
-2.0
0.0
2.0
4.0
Discriminant Function 3

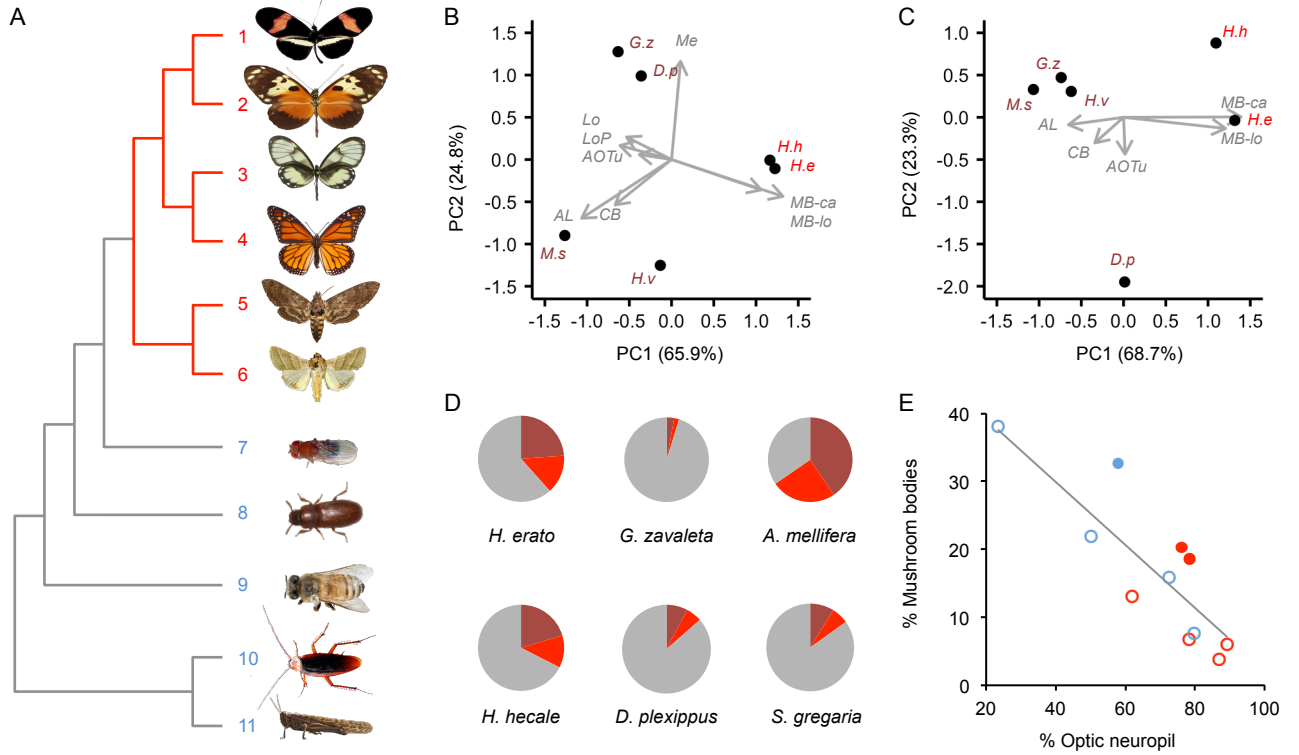
A
1
2
3
4
5
6
7
8
9
10
11
B
G.z
Me
D.p
Lo
LoP
AOTu
H.h
H.e
MB-ca
MB-lo
AL
CB
M.s
H.v
PC2 (24.8%)
PC1 (65.9%)
C
H.h
G.z
M.s
H.v
MB-ca
AL
H.e
MB-lo
CB
AOTu
D.p
PC2 (23.3%)
PC1 (68.7%)
D
H. erato
G. zavaleta
A. mellifera
H. hecale
D. plexippus
S. gregaria
E
% Mushroom bodies
% Optic neuropil